(List of publications)

List of papers communicated/accepted/published/presented

Journals

1. Abhinav Srivastava, Nayan Kr. Debnath, Vijay Kumar, P. Hemanth Kumar, Vinay Kumar Singh, "The effect of mechanochemically activated MgO in Al_2O_3–MgO–C refractory. Part I: Formulation and Properties", ***Ceramics International***, 42, 10116–10121, (2016),

2. Abhinav Srivastava, Vinay Kumar Singh, Vijay Kumar, P. Hemanth Kumar, "Auto combustion processed high alumina cement and mechanochemically synthesized cordierite based low cement castable: formulation and properties", ***Ceramics International***, 40(9A),14061-14072, (2014).

3. Abhinav Srivastava, Vinay Kumar Singh, Vijay Kumar, P. Hemanth Kumar, Himanshu Tripathi, Ashish Chaudhary, Krit Asiwal, Rahul Pandey, Shyam Kumar Suman "Some studies on ceria–zirconia reinforced solvothermally synthesized cordierite nano-composites", ***Journal of Alloys and Compounds***, 586(3), 581–587, (2014).

4. Abhinav Srivastava, Vijay Kumar, V. K. Singh, "A Review on the Implementation High Carbon Binders in Refractories Technology", ***Anvikshiki***, 6(2), 58-62, (2012).

5. Abhinav Srivastava, Nayan Kr. Debnath, Vijay Kumar, P. Hemanth Kumar, Vinay Kumar Singh, "Effect of antioxidant particle size in Al_2O_3-ZrO_2-C refractories", ***Ceramics International***, [Minor Revision submitted].

Conferences

1. Abhinav Srivastava, Vijay Kumar, V.K. Singh, and S. Singh, "Sintering Studies of Combined Gelation-Precipitation Processed Al_2O_3-ZrO_2 Nano-composites", ***National Symposium on Ceramics: Energy and Environment***, 204-208, (11-13 Jan 2011) Kolkata.

2. Abhinav Srivastava, Vijay Kumar, Vinay Kumar Singh, "Effect on mechanical properties of solvothermally synthesized cordierite and ceria stabilized zirconia nano composites", ***4th International Conference on Recent Advances in Composite Materials***, 134-142, (18-21 Feb. 2013), Goa.

3. Abhinav Srivastava, Vijay Kumar, Vinay Kumar Singh, "Slag Resistance Behaviour of Gelation and Co-Precipitation Processed Nano-Crystalline Spinel-Carbon Refractory", ***International Conference on Advances in Refractories and Clean Steel Making***, (26-28 June 2013), SAIL Ranchi.

4. Abhinav Srivastava, Vijay Kumar, A. Sampath Kumar, Shyam Kumar Suman, Shubham Jain and Vinay Kumar Singh, "Zircon Reinforced Two Step Re-Crystallized Cordierite Nano-Composite: Synthesis and Characterization", ***International Conference on Advances in Refractories and Clean Steel Making***, (26-28 June 2013), SAIL Ranchi.

5. Abhinav Srivastava, Vijay Kumar, Vinay Kumar Singh, P. Hemanth Kumar, "Synthesis and studies on cordierite based high alumina low cement castable", ***77th Annual Session and International Conference of Indian Ceramic Society***, (19-20 Dec. 2013), Bistupur, Jamshedpur.

6. Abhinav Srivastava, Vijay Kumar, Himangi Singh, P. Hemanth Kumar, V. K. Singh "Some studies on Ceria–Zirconia reinforced mechanochemically activated cordierite nano-composites", ***Behind the Teacher's Desk***, (27-28 March 2014), NML Jamshedpur.

7. Abhinav Srivastava, Vijay Kumar, P. Hemanth Kumar, Vinay Kumar Singh, "Particle size or amount of antioxidants: Which mostly affects the durability of Al_2O_3-ZrO_2-C refractories?", ***78th Annual Session and International Conference of Indian Ceramic Society***, (02-03 Feb. 2015), Bistupur, Jamshedpur.

8. Abhinav Srivastava, Nayan Kr Debnath, Vijay Kumar, P. Hemanth Kumar, Vinay Kumar Singh, "How Much *in situ* Spinelization is Sufficient for a Better Slag Resistance Behavior of Al_2O_3-MgO-C?", ***78th Annual Session***

and International Conference of Indian Ceramic Society, (02-03 Feb. 2015), Bistupur, Jamshedpur.

9. Abhinav Srivastava, Vinay Kumar Singh, "Comparative study of carbon source on MgO-Al_2O_3-C refractory: Part I. Slag Attack, Oxidation Resistance and Mechanical Properties", ***79th Annual Session and International Conference of Indian Ceramic Society***, (15-17 Feb. 2015), Bangalore.

(List of papers communicated/accepted/published/presented)

Ceramics International 42 (2016) 10116–10121

Contents lists available at ScienceDirect

Ceramics International

journal homepage: www.elsevier.com/locate/ceramint

The effect of mechanochemically activated MgO in Al_2O_3–MgO–C refractory. Part I: Formulation and properties

Abhinav Srivastava*, Nayan Kr. Debnath, Vijay Kumar, P. Hemanth Kumar, Vinay Kumar Singh

Department of Ceramic Engineering, IIT (BHU), Varanasi 221005, India

ARTICLE INFO

Article history:
Received 5 March 2016
Accepted 16 March 2016
Available online 21 March 2016

Keywords:
A. Milling
B. X-ray methods
C. Thermal expansion
D. Spinels
E. Refractories

ABSTRACT

Steel-making processes associate with highly corrosive slag and aggressive reactions giving rise to erosive conditions. *In-situ* spinel ($MgAl_2O_4$) shows good slag resistance in Al_2O_3–MgO–C (AMC) secondary refining ladles because spinel has an excellent cation absorption capacity from the slag due to the void spaces in its crystal structure. The aim of our research work was the optimization of *in-situ* spinel formation in AMC refractory and to minimise the crack and rupture through residual expansion. Mechanically activated reactive magnesia was added up to 10 wt% in different proportions into the starting raw material batches, which comprised of graded fused alumina and flake graphite. A resol type resin was used as a thermosetting binder, and a combination of Al-B_4C fine powder was used as an antioxidant. Prepared briquettes by the cold pressing of these batches were first cured in an oven at resin transition temperature for its polymerization. The samples were then coked at 1400 °C. The quantitative crystallinity was studied using X-ray diffraction patterns. The coefficient of thermal expansion was determined by dilatometric analysis and evaluation of microstructural cracks was examined by SEM.

1. Introduction

Refractory applications are becoming more distinct due to the increased cost and waste associated with a one-size-fits-all approach. It creates the need for an in-depth understanding of refractory behaviour in the presence of minor elements. Al_2O_3–MgO–C is increasingly being used in refractories for secondary steel-making especially for ladle applications due to their particular combination of resistance to slag corrosion, high thermal shock resistance and excellent hot strength. Al_2O_3–spinel refractories usually show better thermal shock/spalling resistance than MgO–spinel refractories as the difference in thermal expansion coefficients of the former is lower than later [1].

M. Bavand-Vandchali et al. suggest the nature of *in-situ* spinel in Al_2O_3–MgO–C refractory matrix produces an interlocking texture, which holds the graphite flakes within and improves the structural integrity. In this type of skeletal structure, the graphite and antioxidants can be confidently increased for getting better wear resistance [2]. E.Y. Sako et al. addressed that principal aspects of the better corrosion and slag penetration resistance are the replacement of pre-formed spinel by *in-situ* spinel refractory [3]. In a later article, they reported that *in-situ* spinel expansion control by adding reactants with nano sizes provided the lowest expansion [4]. However, the expansion and the performance at high temperatures of the refractory designed by micrometric-sized Al_2O_3 and MgO particles were almost as suitable as the nano Al_2O_3.MgO composition [5]. It brings us to the fact that use of nano-materials can be industrially avoided until the time, its cost is reduced, or its performance can be optimised more economically.

A graphite content of the order of 6 wt% in the refractory matrix apparently helps build an appropriate set of thermo-mechanical properties and higher corrosion resistance, due to the low thermal expansion coefficient, high thermal conductivity, high refractoriness and a non-wettability by the slag [6]. The refractory containing coarser MgO grains usually present reduced corrosion behaviour, owing to the higher residual expansion, which helps the physical slag infiltration. Nonetheless, in an expansion controlled conditions, the penetration indexes were reduced as a result of the lower volume of pores and flaws closure in the refractory microstructure [7].

High expansion of *in-situ* spinel formation needs optimization. Some expansion on the hot side of use is desired because it can close joints and cracks. However, too much expansion can lead to spalling or even damage to the steel shell of the ladle [8].

Although the abrasion and corrosion resistance is one of the chief requisites for refining ladles, conclusive statements about the contents of *in-situ* spinelization in AMC have not been reported.

* Corresponding author.
E-mail address: srivasbhinav@gmail.com (A. Srivastava).

http://dx.doi.org/10.1016/j.ceramint.2016.03.121
0272-8842/

Table 1
Chemical composition of different batches.

Raw Materials	AMC1	AMC2	AMC3	AMC4	AMC5	AMC6
WFA (0.2–3 mm)	72	72	72	72	72	72
WFA (74–44μ)	15	13	11	9	7	5
MgO (44μ)	0	2	4	6	8	10
Flaky graphite	7	7	7	7	7	7
Resol type Liq. resin	3.50	3.50	3.50	3.50	3.50	3.50
Powder resin	0.50	0.50	0.50	0.50	0.50	0.50
Nano-carbon black	1.0	1.0	1.0	1.0	1.0	1.0
Al-metal powder	0.50	0.50	0.50	0.50	0.50	0.50
B_4C	0.50	0.50	0.50	0.50	0.50	0.50

Considering this aspect, the primary aim of this work was to obtain an optimum content of *in-situ* spinel for high thermo-mechanical properties. Fine mechanochemically activated MgO was varied 0–10 wt% in AMC refractory. A quantitative XRD technique was used to deduce the percentage of *in-situ* spinelization. A dilatometer analysis followed by microstructural evaluation through SEM was carried out to identify micro-cracks developed.

2. Materials and methods

2.1. Raw materials

The high purity white fused alumina (99%, Almatis, Kolkata, India) with different size fraction (3–0.2 mm and 44–74 μ) was used as the matrix component. A thermosetting resol type liquid and powder resin were used as a binder and additional source of carbon (Fortis Chemicals Pvt. Ltd., Jharsuguda, India). Natural flake 97FC grade graphite (97 % fixed carbon) and nano carbon black (Birla Carbon) were used as carbon sources. Fine reactive magnesia powder (Almatis) was used as additive. Aluminium metal powder (Loba Chemicals Pvt. Ltd, Mumbai, India) and boron carbide powder (Vajrabor, Bhukhanvala Industries Pvt. Ltd. Mumbai, India) were used as antioxidants in the system.

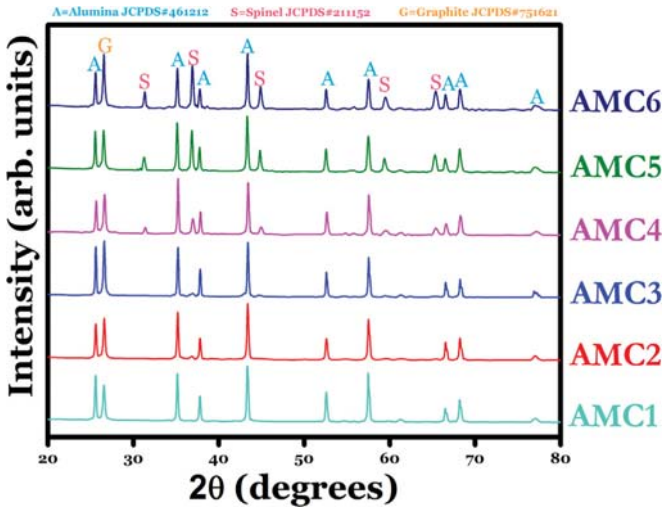

Fig. 2. XRD analysis of AMC sample coked at 1400 °C with 3 h soaking.

Table 2
Relative crystallinity (%).

Sample Code	Relative crystallinity %		
	Al_2O_3	$MgAl_2O_4$	Graphite
AMC1	89.15	–	10.85
AMC2	87.66	4.54	11.80
AMC3	75.64	10.76	13.60
AMC4	67.59	21.86	10.55
AMC5	65.06	26.89	8.05
AMC6	55.37	34.90	9.71

2.2. Methods

The raw materials play a vital role in the performance and life of the refractories. The size of the raw materials is selected from Andreassen equation which gives the Cumulative Volume Percentage Finer than (CPFT).

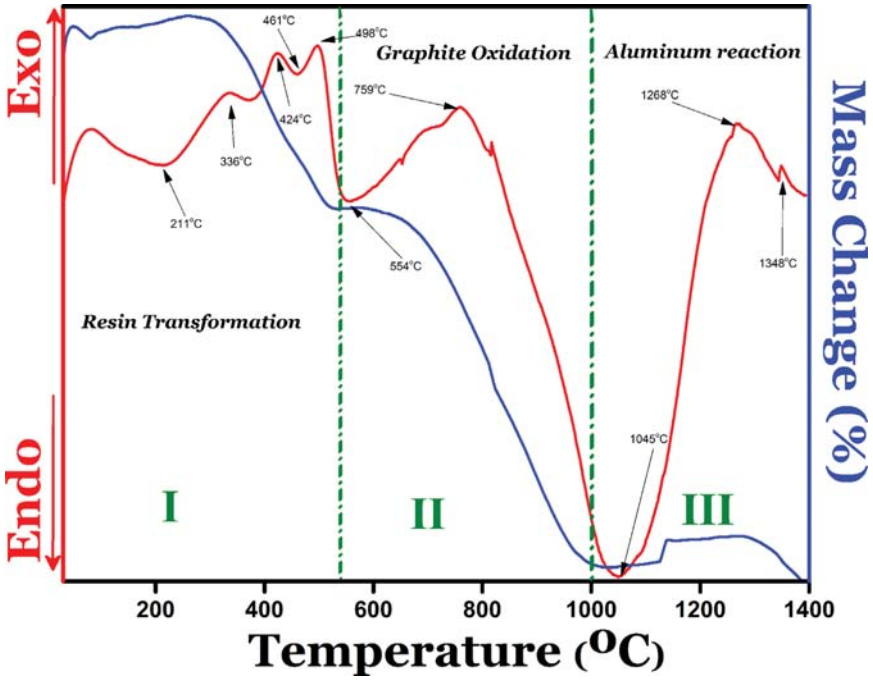

Fig. 1. Thermal evolution of AMC4 specimen.

Table 3
Crystallite size, dislocation density and micro strain.

Sample	Crystallite size (*D*) nm			Dislocation density (δ) line^2/m^2 ($\times 10^{15}$)			Micro strain ε ($\times 10^{-3}$)		
	Al_2O_3	$MgAl_2O_4$	Graphite	Al_2O_3	$MgAl_2O_4$	Graphite	Al_2O_3	$MgAl_2O_4$	Graphite
AMC1	38.61	–	30.55	0.671	–	1.071	0.897	–	1.134
AMC2	39.591	34.622	17.537	0.637	3.251	0.834	0.875	1.975	1.001
AMC3	45.383	8.805	36.857	0.485	12.898	0.736	0.763	3.935	0.940
AMC4	46.510	23.537	31.872	0.462	1.804	0.984	0.744	1.472	1.087
AMC5	39.526	32.847	32.863	0.640	0.926	0.925	0.876	1.054	1.054
AMC6	42.528	33.693	34.897	0.552	0.880	0.821	0.814	1.028	0.992

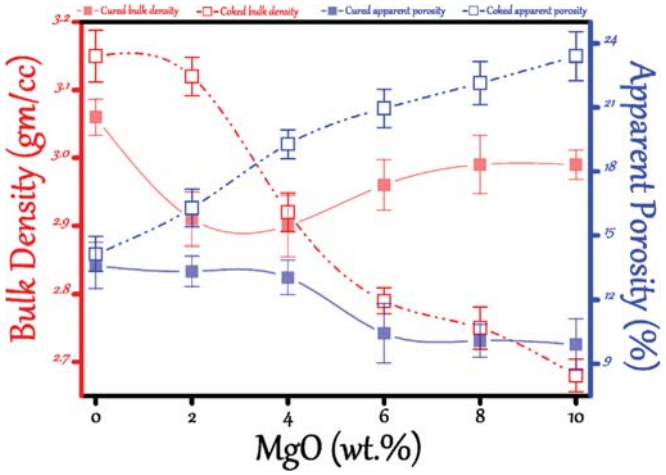

Fig. 3. Bulk Density and apparent porosity of AMC refractories after curing at 200 °C and coking at 1400 °C.

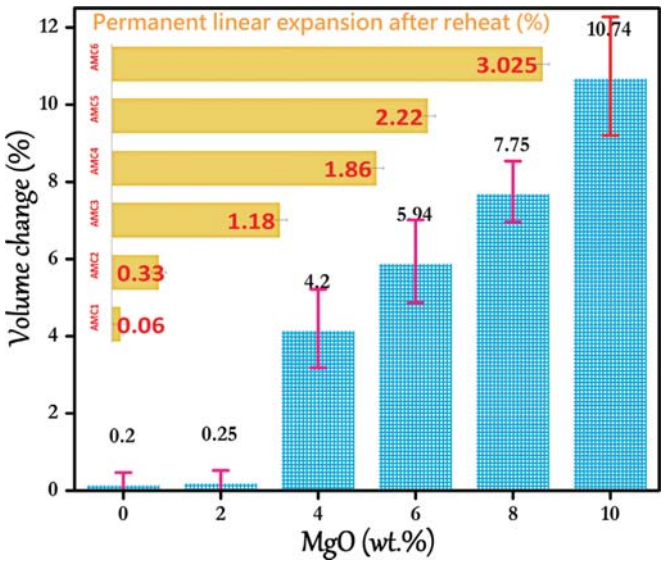

Fig. 4. Volumetric expansion and Permanent linear change after one heat cycle as a function of magnesia content.

$$\mathrm{CPFT}=\left(\frac{d}{D}\right)^{q} \quad (1)$$

where '*d*' is particle size, '*D*' is maximum particle size and '*q*' is the distribution coefficient. The MgO as obtained was mechanochemically activated in a high energy planetary ball mill at a constant 600 rpm for 1 h. Ball and jar were made of TiC coated stainless steel. The ball to powder ratio was kept 4:1. The composition details are given in Table 1. An impeller type high-speed mixer was used to homogenise the resin and raw materials of the batch for 15 min. Subsequently, the batches were kept for 2 h room temperature aging. According to ASTM standards of CMOR, HMOR and dilatometric analysis, samples were cold pressed under a constant 200 MPa pressure using a uniaxial hydraulic press. Tempering of the pressed green bricks was done at 200 °C for 24 h (for polymerization and development of carbon-carbon bonds in the resin). The test samples were coked at 1400 °C in an electric furnace with a dwell time of 3 h at a heating rate of 5 °C.

2.3. Characterization

Powder X-ray diffraction patterns of AMC1-6 coked at 1400 °C were recorded using a Rigaku portable high-resolution powder X-ray diffractometer employing Cu Kα1 radiation and Ni-filter. Phase identification analysis was carried out by comparing the respective powder XRD patterns with the standard database stated by JCPDF. Detailed studies of the phase formation and changes in the temperature range and variation in compositions were carried out.

Apparent porosity (A.P.) and bulk density (B.D.) were determined according to ASTM C20-00 [9]. Three-point bending strength tests were performed as cold and hot modulus of ruptures (CMOR, HMOR) according to ASTM C133-97 and C1099 – 07 respectively [10,11].

The thermal expansion of the material was determined by dilatometer (supplied by VB Ceramic Consultants, India) in the temperature range 20–1400 °C at 6 °C/min. The dilatometer was equipped with SiC heating element with a control accuracy of ± 1 °C. It had a Nippon PID programmable digital temperature indicator cum controller. The samples for the coefficient of thermal expansion (CTE) measurement were cut and polished uniformly to the size of 45 × 15 × 10 mm. This firing was done in an electric furnace containing SiC heating elements. These samples were also analysed by an FESEM ZEISS SUPRA™ 40 instrument operated at 5 kV for their surface cracks.

3. Results and discussion

The thermograms acquired by DTA-TGA of AMC4 is shown in Fig. 1. The DTA plots show peaks between 200 and 580 °C that are ascribed to the resin transformation [12,13] and residual carbon (glassy-carbon) oxidation around 554 °C. However, the resin pyrolysis temperature is also affected by the existence of diverse inorganic components [14]. Weight loss accompanies both processes concerning the resin carbonization and the oxidation of the residual carbon due to the evolution of gases.

The diffractograms of the AMC briquettes are plotted in Fig. 2, and the identified phases are indicated on the graph along with the JCPDF files used. The major phases of each formulation are corundum (α-Al_2O_3) and graphite. The presence of metallic aluminium, B_4C is not detected due to them being below the

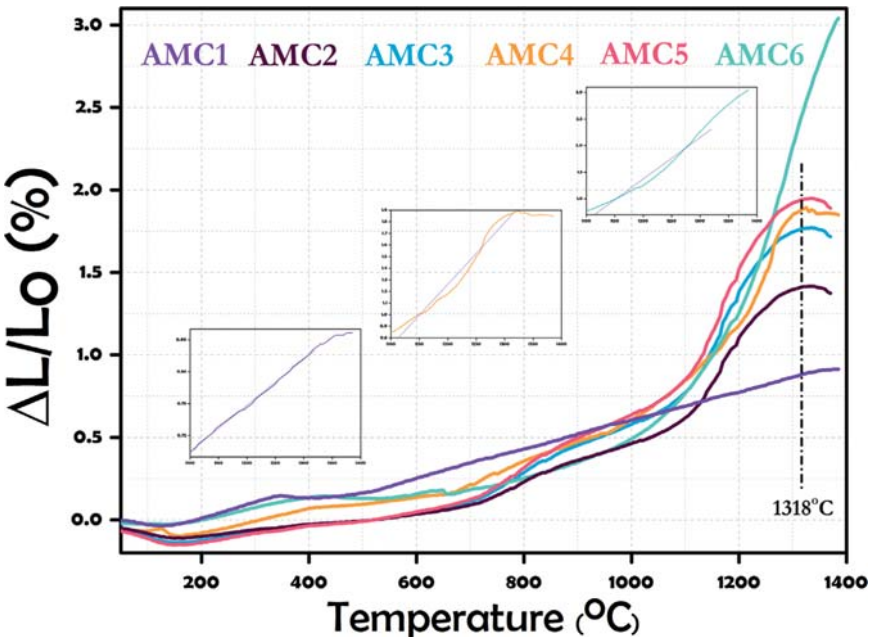

Fig. 5. Coefficient of thermal expansion behaviour of different AMC refractories; inset figures represent linear fits drawn on AMC1, AMC4 and AMC6.

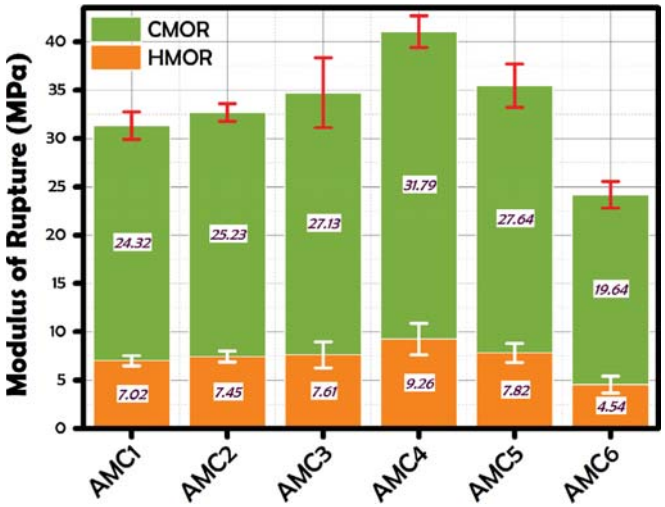

Fig. 6. Cold and Hot modulus of rupture of different AMC refractories.

detection level of XRD (< 5 wt%). From the graph, it is evident that in AMC2 spinel formation starts and is maximum in AMC6. Relative crystallinity of the individual phases present was calculated with the help of commercially available software Origin 8.5 using the formula below [15].

$$\text{Relative crystallinity}(\%) = \frac{\sum (I \times \beta)\text{desired phase}}{\sum (I \times \beta)\text{all phases}} \times 100 \quad (2)$$

where I is the peak intensity and β is full width at half maximum. Calculations indicate a quantitative phase of the sample have 4.5, 10.7, 21.8, 26.8 and 34.9 % *in-situ* spinel for AMC2, AMC3, AMC4, AMC5 and AMC6 respectively more details are enlisted in Table 2. The crystallite size (D), microstrain (ε) and dislocation density (δ) were also evaluated [15] and is listed in Table 3.

The bulk density and apparent porosities of the samples are portrayed in Fig. 3. It can be observed that AMC1 had maximum density both cured and coked. Its corresponding apparent porosity is around 13% being almost same for both cured and coked. As fine magnesia content increases in the matrix, the apparent porosity of cured samples rapidly decreases which becomes constant after a

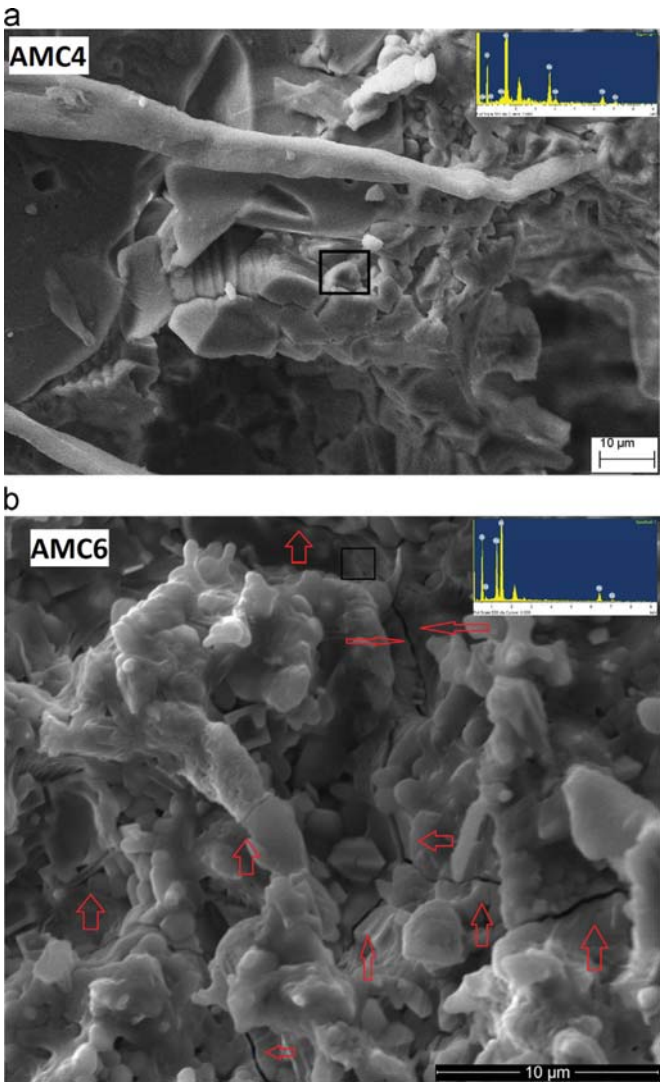

Fig. 7. Microstructure of (a) AMC4, (b) AMC6.

6 wt% magnesia addition. It brings us to a fact that there is a certain limit to which micro-fine inclusions may help in diminishing the porosity and, in this case, it is 6 wt% (AMC4) [16,17]. Here we can see that the cured bulk density initially decreases and then increases which reciprocate the trend followed by coked samples. The formation of new ceramic phase with a lower relative density (spinel) might be the cause for it; this phenomenon is absent in cured samples. The AMC6 has an apparent coked porosity of around 24% owing to *in-situ* spinelization followed by volumetric expansion. The path taken by the evolution of gaseous products is also responsible for increased coked porosity.

The variation in the percent volumetric change after the first firing and permanent linear change (PLC) after reheating are studied in Fig. 4. The AMC1 and AMC2 samples show minor volume changes demarcating that alumina, carbon and rest other do not contribute much to expansion. The samples AMC3-6 illustrates an expansive tendency which confirms that all the expansion is dependent on the amount of magnesia present. The primary contributor to residual expansion is spinel formation, which continues to increase even after reheating [18]. The AMC6 has a PLC value of 3.02 %; this huge dramatic expansion may lead to catastrophic failures during use. It also suggests that other than increasing magnesia content, spinel formation is also dependent on the number of firing cycles or soaking periods. Hence, this study suggests that a content of ~21 wt% spinel formation (AMC4) is optimum for this category of refractory.

In Fig. 5, the dilatometric curve of AMC1 is almost linear, progressive and different from rest others. AMC2-5 has a similar incremental slope depending upon the transformations undergone by the materials as the temperature increases. At temperature $< 200\ ^{\circ}C$, volumetric contraction occurs in all the six AMC refractories ascribing to resin transformation. It might be well correlated with increased coked density phenomenon. There is another decrement in the slope of the curves at 650 °C where the glassy carbon starts oxidizing resulting in the formation of gaseous products. The sudden increase in slope at 1100 °C demarcates that the spinel formation has started. This expansion can counteract wear on the joints between the refractory bricks. Furthermore, this expansion also results in micro-cracking due to the difference between coefficients of thermal expansion of the product and reagents, which could lead to enforcement mechanisms. However, these micro-cracks can also become entry points for chemically aggressive slags; therefore, the spinel formation reaction must be controlled and the inclusion of magnesia needs to be optimised. The sample AMC2-5 exhibits a negative slope after 1318 °C due to liquid phase sintering followed by a quick densification. The inset demonstrates the linear fit of the AMC1, AMC4 and AMC6 curves in the temperature range 1100–1318 °C. The corresponding slopes for AMC1, AMC4 and AMC6 have values $8.65 \times 10^{-4}\ ^{\circ}C^{-1}$, $5.31 \times 10^{-3}\ ^{\circ}C^{-1}$ and $7.82 \times 10^{-3}\ ^{\circ}C^{-1}$ respectively. The AMC6 sample shows abnormally high CTE ascertaining unfit for application viewpoint.

Hot and cold modulus of rupture is displayed in Fig. 6. It can be noted that there is a significant 23.4% increase in CMOR value after a 6 wt% magnesia inclusion although there is a noteworthy decrement after 10 wt% magnesia addition. Similarly, the HMOR values depict a 24.1% growth and 35.3% decline in AMC4 and AMC6 respectively. The microporosity due to the alignment of materials creates foundations for crack deflection and diversity in the matrix, helps in accommodating external mechanical constraint. The expansion of materials with temperature is natural but in a heterogeneous microstructure as this composition, and disparate CTE caused excessive stress gradients inside AMC6 triggering its self-destruction with rising temperature. The alumina-based refractories are known to exhibit superplastic behaviour at high temperatures in the presence of ultrafine spinel grains [19]. When the temperature was raised, and a tensile stress was applied, the grain boundary sliding might have occurred impeding the abnormal grain growth of alumina thereby increasing the hot rupture strength.

Fig. 7(a, b) are the photomicrographs of a coked AMC4 and AMC6 specimen. The Fig. 7(a) is a dense microstructure; free from any visible crack. The formation of micro-cracks is visible in Fig. 7 (b), even though a free expansion might have occurred as it was not lined in a refractory. These cracks are inelastic; however, linear thermal expansion is reversible in nature hence upon cooling the joint structure will tend to open. So for a successful lining, it would be wise to use lower amounts of magnesia. EDX analysis in the inset mark the existing elements in the right proportion, indicating that the specimen is primarily composed of aluminium, magnesium, oxygen and carbon.

4. Conclusion

This paper proposes a comprehensive approach to evaluating the limiting value of magnesia in Al_2O_3–MgO–C refractory. The thermal analysis distinguishes the weight loss from the combustion of the resin. The X-ray diffraction has proven to be a simple, practical and accurate tool for the quantitative determination of the mineralogical composition. The density and porosity are found to be dependent on micro-fine additions and *in-situ* spinelization. Linear dimensional changes continue to occur after reheat and dilatometric analysis establish that its chief cause is spinel formation. The structural defects in AMC6 by forming of $MgAl_2O_4$ lead to continuous crack which further result in the destruction of the sample by load bearing stress at high temperature.

References

[1] S. Zhang, W.E. Lee, Spinel-containing refractories, in: Charles A. Schacht (Ed.), Refractories Handbook, Marcel Dekker, Inc., New York, 2004, pp. 215–258.
[2] M. Bavand-Vandchali, H. Sarpoolaky, F. Golestani-Fard, H.R. Rezaie, Atmosphere and carbon effects on microstructure and phase analysis of *in situ* spinel formation in MgO–C refractories matrix, Ceram. Int. 35 (2009) 861–868.
[3] E.Y. Sako, M.A.L. Braulio, V.C. Pandolfelli, The corrosion and microstructure relationship for cement-bonded spinel refractory castables, Ceram. Int. 38 (2012) 2177–2185.
[4] E.Y. Sako, M.A.L. Braulio, V.C. Pandolfelli, How effective is the addition of nanoscaled particles to alumina–magnesia refractory castables? Ceram. Int. 38 (2012) 5157–5164.
[5] W.S. Resende, R.M. Stoll, S.M. Justus, R.M. Andrade, E. Longo, J.B. Baldo, E. R. Leite, C.A. Paskocimas, L.E.B. Soledade, J.E. Gomes, J.A. Varela, Key features of alumina/magnesia/graphite refractories for steel ladle lining, J. Eur. Ceram. Soc. 20 (2000) 1419–1427.
[6] M. Bag, S. Adak, R. Sarkar, Study on low carbon containing MgO–C refractory: Use of nano carbon, Ceram. Int. 38 (2012) 2339–2346.
[7] E.Y. Sako, M.A.L. Braulio, V.C. Pandolfelli, Al_2O_3–MgO castables performance in an expansion constrained environment, Ceram. Int. 38 (2012) 3513–3518.
[8] M.A.L. Braulio, M. Rigaud, A. Buhr, C. Parr, V.C. Pandolfelli, Spinel-containing alumina-based refractory castables, Ceram. Int. 37 (2011) 1705–1724.
[9] ASTM C20-00(2010) Standard Test Methods for Apparent Porosity, Water Absorption, Apparent Specific Gravity, and Bulk Density of Burned Refractory Brick and Shapes by Boiling Water.
[10] ASTM C133 − 97 (Reapproved 2008) Standard Test Methods for Cold Crushing Strength and Modulus of Rupture of Refractories.
[11] ASTM C1099 − 07 (Reapproved 2012) Standard Test Method for Modulus of Rupture of Carbon-Containing Refractory Materials at Elevated Temperatures.
[12] V. Muñoz, A.G. Tomba Martinez, Thermomechanical behaviour of Al_2O_3–MgO–C refractories under non-oxidizing atmosphere, Ceram. Int. 41 (2015) 3438–3448.
[13] V. Muñoz, A.G. Tomba Martinez, Thermal evolution of Al_2O_3–MgO–C refractories, Procedia Mater. Sci. 1 (2012) 410–417.
[14] V. Muñoz, P. Pena, A.G. Tomba Martínez, Physical, chemical and thermal characterization of alumina–magnesia–carbon refractories, Ceram. Int. 40 (2014) 9133–9149.
[15] P.H. Kumar, A. Srivastava, V. Kumar, P. Kumar, V.K. Singh, Effect of high-energy ball milling and silica fume addition in $BaCO_3$–Al_2O_3. Part I: formation of cementing phases, J. Am. Ceram. Soc. 97 (12) (2014) 3755–3763.
[16] A. Srivastava, V. Kumar Singh, V. Kumar, P. Hemanth Kumar, V.K. Singh, P.

H. Kumar, Low cement castable based on auto combustion processed high alumina cement and mechanochemically synthesized cordierite: formulation and properties, Ceram. Int. 40 (2014) 14061–14072.
[17] A. Srivastava, V.K. Singh, V. Kumar, P. Hemanth Kumar, H. Tripathi, A. Chaudhary, et al., Some studies on ceria–zirconia reinforced solvothermally synthesized cordierite nano-composites, J. Alloy. Compd. 586 (2014) 581–587.
[18] V. Muñoz, P.G. Galliano, E. Brandaleze, A.G. Tomba Martinez, Chemical wear of Al_2O_3–MgO–C bricks by air and basic slag, J. Eur. Ceram. Soc. 35 (2015) 1621–1635.
[19] P.H. Kumar, A. Srivastava, V. Kumar, V.K. Singh, Implementation of industrial waste ferrochrome slag in conventional and low cement castables: effect of calcined alumina, J. Asian Ceram. Soc. 2 (2014) 371–379.

Available online at www.sciencedirect.com

ScienceDirect

Ceramics International 40 (2014) 14061–14072

CERAMICS INTERNATIONAL

www.elsevier.com/locate/ceramint

Low cement castable based on auto combustion processed high alumina cement and mechanochemically synthesized cordierite: Formulation and properties

Abhinav Srivastava*, Vinay Kumar Singh, Vijay Kumar, P. Hemanth Kumar

Department of Ceramic Engineering, Indian Institute of Technology (BHU), Varanasi, India

Received 2 December 2013; received in revised form 29 May 2014; accepted 29 May 2014
Available online 6 June 2014

Abstract

Nano high alumina cement was prepared by an auto combustion method which was a self-propagating high temperature synthesis. Metal nitrate precursors were used in this process and thermal reactions were done at 1000 °C. Prepared high alumina cement was tested for its cementing properties and mechanical behavior. These properties were compared with commercialized CA-25 C high alumina cement. In a separate process, cordierite was mechanochemically synthesized by mixing proper amounts of kaolin, talc and gibbsite and then grinding in a high-speed planetary mill to reduce the initial particle sizes of mixes. The prepared mixes were calcined at different temperatures. In order to study the effects of process variables, the powders were analyzed by XRD and SEM. Based on XRD results it was concluded that the cordierite mixture was amorphous to XRD by high energy grinding of the mixes at 600 rpm for 30 min. Cordierite was successfully produced at temperatures as low as 1150 °C. Low cement castables were formulated introducing the prepared HAC as a binder phase in the cordierite matrix with further addition of silicon carbide for enhancing mechanical properties. Formulated LCC briquettes were analyzed for their physico-mechanical properties including bulk density, apparent porosity, cold crushing strength and cold modulus of rupture.

Keywords: A. Milling; C. Thermal shock resistance; D. Cordierite; D. SiC

1. Introduction

The synthesis of nanostructured materials has generated great expectations to develop newer technological products in the past few years. Because of the extremely small dimensions, a large fraction of atoms in these materials are situated at grain boundaries or their interfacial interaction is extremely higher than bulk coarse-grained materials [1–3]. Thermal reactions between these nanomaterials are possible at lower temperatures. Advantages of nanocrystalline materials are their superior phase homogeneity, superior sinterability and new microstructures providing unique mechanical, electrical, dielectric, magnetic, optical and catalytic properties [4–6].

High alumina cement is used as binding material for monolithic applications and a significant advancement in monolithic technology is the development of refractory concretes or castables. Castables are complex refractory formulations consisting of refractory cement, high-quality precision-sized aggregates, fillers, binders and other additives. The use of reduced cement contents in monolithic such as low cement castables (LCCs) and ultra-low cement castables (ULCCs) has increased significantly in industries for kiln construction and repairing works over the last couple of decades. These castables may be cast in molds to form specific products (pre-cast shapes) or cast "in place", as when forming a lining for a kiln furnace. The main technical advantages of LCCs and ULCCs are their excellent physical properties such as high density, low porosity, high cold/hot strengths, high abrasion, and corrosion resistance [2]. There have been a rapid development in the use of nanostructured low cement castables in

*Corresponding author.
E-mail address: srivasabhinav@gmail.com (A. Srivastava).

http://dx.doi.org/10.1016/j.ceramint.2014.05.134
0272-8842/

many industries such as non-ferrous metals, cements, petrochemicals and of course in iron and steel industries [1,2]. Because of their superior properties, the low cement castables (LCC's) helped the iron and steel makers to reduce the consumption of refractories and hence lowering their operating cost [3]. The high alumina cement used as a hydraulic binder at current work was synthesized by the auto combustion reaction of redox mixtures of the corresponding water soluble nitrate salts with urea [6,7]. The method was exothermic in nature and there was a very rapid and self-sustaining chemical reaction. Its key feature is that the heat required to drive the chemical reaction is provided by the reaction itself and not by the external sources [8–10].

In refractory technology, cordierite ($2MgO \cdot 2Al_2O_3 \cdot 5SiO_2$) is one of the most interesting phases of the system $MgO–SiO_2–Al_2O_3$ [11–13]. Cordierite ceramics have a low thermal expansion coefficient, excellent thermal shock resistance, low dielectric constant, and high chemical and mechanical durability [9,10,14]. Due to its lower processing costs and its good electrical properties, cordierite is an alternative material to be used as substrate in replacement of alumina in electronic industries [5,12]. Cordierite is the best material for kiln furniture due its low thermal expansion coefficient. The main drawback of this material is its low fracture toughness, which limits its structural applications. Another problem in refractories industries is to manufacture pure cordierite phase as it is always accompanied by a spinel ($MgAl_2O_4$) phase, which impairs the thermal shock resistance of end product due to its high thermal expansion coefficient [4]. Cordierite melts incongruently at 1460 °C. It then changes into mullite and liquid phase [13], [14,15]. It has different polymorphic forms. One phase is α-cordierite having hexagonal symmetry. This phase is retained if the fast crystallization occurs in the temperature range of 1000–1300 °C. β-cordierite of a rhombic structure can be produced by crystallization under 950 °C. Another phase, a metastable form (μ-cordierite), can be produced by devitrification of cordierite glass under 925 °C [16]. Cordierite masses always have a very narrow sintering interval, which is one of the basic problems in production of cordierite ceramics [4,14,16]. Cordierite masses composed of kaolin, talc and technical silica can have only 10–20 °C variation in their sintering temperature, which makes the products very sensitive to sintering as well as to their properties [5,17,18]. This is the main reason why they are not easily sintered to obtain pure cordierite phase without any sintering aids in order to avoid a liquid-phase close to their melting point [19,20].

Preparation of cordierite through solid state reaction sintering is the most common method for cordierite preparation [5]. One of the problems derived from the use of natural raw materials in solid state reactions is of their coarse particle size distribution that lowers the thermal reactivity. The other methods of cordierite preparation are sol–gel [12], combustion synthesis [13], mechanochemical (by talc, kaolinite and boehmite) [14] and co-precipitation [15]. The temperature required for cordierite formation through solid state reactions is ~1400 °C whereas it can be made at lower temperatures through wet chemical methods. Doping of silicon carbide in cordierite formation has also been extensively studied. It is found that this material not only enhances the cordierite formation, but it improves structural strength and fracture toughness [21–24].

In the present work mechanochemical synthesis was used for the formation of cordierite at low temperatures. During mechanical activation, precursor materials lost their crystallinity and this improved their reactivity [14]. The milling effects on cordierite formation were studied with different milling time and rotational speed. The amount of total cordierite formation was found to be dependent on milling parameters. In particular, there have been no studies on the mechanical response of cordierite castables under cyclic thermal shocks [25,26]. Therefore, the cordierite samples were tested for their thermal behavior. Physico-mechanical properties as a function of temperature of cordierite based castables using prepared high alumina cement were also investigated. Formulated castable reinforced with silicon carbide as whiskers and granules were also the main focus of this study. The formulation of fine grained cordierite based castables in the above manner proved to be a good refractory material. It may be one of the most ideal candidates for hot-gas or molten-metal filters, catalytic supports, thermal insulators, kiln furniture and complex refractory shapes referring to burner tips.

2. Materials and methods

2.1. Materials

AR grade kaolin ($Al_2O_3 \cdot 2SiO_2 \cdot 2H_2O$), talc ($3MgO \cdot 4SiO_2 \cdot H_2O$), and gibbsite ($Al(OH)_3$) provided by Loba Chemie Pvt. Ltd., Mumbai, India, used as raw materials for cordierite synthesis. Hydrated aluminum nitrate $Al(NO_3)_3 \cdot 9H_2O$ and hydrated calcium nitrate $Ca(NO_3)_2 \cdot 4H_2O$ used for high alumina cement production were also AR grade and procured from Loba Chemie Pvt. Ltd., Mumbai India. CA-25 C high alumina cement used for comparative study was supplied by Almatis, India. Commercially available α-SiC powder (99.4% purity, 10.0 μm, Carborundum Universal Limited, India) and silicon carbide whiskers (98.7% purity, 6.0 μm, Carborundum Universal Limited, India) were used for castable formulations.

2.2. Auto combustion processed high alumina cement

The auto-combustion synthesis techniques involve the process in which saturated aqueous solution of the desired metal salts with a suitable organic fuel is heated to their boiling point. The mixture ignites and a self-sustaining and rather fast combustion reaction takes place. This reaction results in a dry, usually crystalline oxide powder [6,9]. To produce high alumina cement (HAC80), the solution containing the desired metal ions in the form of water soluble nitrate salts and urea as a fueling agent were used [7]. While redox reactions are exothermic in nature and often lead to explosion if not controlled, the combustion of metal nitrates and urea mixtures

usually occurs as a self-propagating and non-explosive exothermic reaction [8]. The large amounts of gases formed can result in the appearance of a flame, which can reach temperatures in excess of 1000 °C [10]. To synthesize high alumina cement via self-propagating high-temperature synthesis, aluminum nitrate $Al(NO_3)_3 \cdot 9H_2O$ and calcium nitrate $Ca(NO_3)_2 \cdot 4H_2O$, as cation precursors and oxidizers, were used. The appropriate amount of these nitrate precursors in 8:2 weight ratio of Al_2O_3/CaO was dissolved in deionized water. For complete dissolution of the salts, the solution was kept on a hot plate at around 60 °C with simultaneous stirring until a clear transparent solution was obtained. In this precursor solution, urea $(NH_2)_2CO$ (99.8% Loba Chemie) as a fuel was then poured keeping a precursor and fuel ratio of 1:1. The prepared gel was dried in an oven at 80 °C to complete dryness. Finally, dried gel powder was calcined for 15 min in air at 500 °C and then quenched to room temperature. A dry, white and very fragile foam was produced in this manner that easily crumbled into fine powder. During the first few minutes of the calcination process, ignition took place with a rapid evolution of large amounts of gases. Therefore, only a small portion of the gel was calcined. The synthesis technique utilized the heat energy released by the redox exothermic reaction at a relatively low ignition temperature between metal nitrates and urea. The process lasted for a relatively short time, so that the particles could be maintained to the nanometer scale. Further this white powder was heat treated at 800–1000 °C in a platinum dish using an electric furnace at a heating rate of 5 °C/min for a holding period of 1 h. The furnace was equipped with SiC heating element and a programmer PID528, manufactured by Selectron Process Controls Pvt. Ltd., India. The programmer has the temperature control accuracy of ±1 °C. After heat treatment the HAC powder was stored in desiccator. This final product was termed HAC80. The probable chemical reactions are given below

$$2Al(NO_3)_3 \cdot 9H_2O + Ca(NO_3)_2 \cdot 4H_2O + x\,CO(NH_2)_2 \xrightarrow{\Delta} CaO \cdot Al_2O_3 + x\,CO_2 + (22+2x)H_2O + (4+x)N_2 \quad (1)$$

$$4Al(NO_3)_3 \cdot 9H_2O + Ca(NO_3)_2 \cdot 4H_2O + x\,CO(NH_2)_2 \xrightarrow{\Delta} CaO \cdot 2Al_2O_3 + x\,CO_2 + (40+2x)H_2O + (7+x)N_2 \quad (2)$$

$$14Al(NO_3)_3 \cdot 9H_2O + 12Ca(NO_3)_2 \cdot 4H_2O + x\,CO(NH_2)_2 \xrightarrow{\Delta} 12CaO \cdot 7Al_2O_3 + x\,CO_2 + (174+2x)H_2O + (33+x)N_2 \quad (3)$$

2.3. Mechanochemically synthesized cordierite

Powder mixtures for cordierite were prepared in stoichiometric proportions equivalent to their theoretical molar ratio. The amount of raw materials was proportioned to obtain cordierite composition according to the equation given below

$$4[Mg_3Si_4O_{10}(OH)_2] + 7[Al_2Si_2O_5(OH)_4] + 10Al(OH)_3 \rightarrow 6[Mg_2Al_4Si_5O_{18}] + 33H_2O \quad (4)$$

A typical 250 g batch of mix then consisted of 99.6 g of talc, 64.1 g of kaolin and 86.3 g of gibbsite to obtain stoichiometry of cordierite. These mixtures were then mechanically activated in the planetary ball mill. The jar and grinding media were of titanium carbide coated stainless steel material. At one time 250 g of material was taken in a jar and pulverized with the help of fifty stainless steel balls (Ø:10 mm) as the grinding media. Grinding time (minute) and grinding rotational speed (rate per minute) were the factors used for producing four different batches. These factors were altered from 300 to 600 rpm and 15–60 min. Mechanically activated powder mixtures were calcined at 1250 °C with a soak period of 3 h and at a heating rate of 5 °C/min.

2.4. HAC80 characterization

X-ray diffraction patterns were determined using a Rigaku portable XRD machine (Rigaku, Tokyo, Japan). Powder calcined at 1000 °C termed as "HA80" and commercial CA-25 C were analyzed by XRD to identify and quantify the cementing phases present. Phase identification analysis was carried out by comparing the respective powder XRD patterns with the standard database stated by JCPDF. Detailed studies of the phase formation and changes over the temperature range and variation in compositions were carried out.

2.4.1. Determination of setting time

The prepared HAC powders were mixed with water (0.85*P*), where *P* is the percentage of water required to produce a paste of standard consistency. Standard consistency of a cement paste is defined as consistency which will permit the Vicat Plunger to a point 5–7 mm from the bottom of the Vicat mold [27]. In present case *P* was calculated to be 27 wt%.

2.4.2. Initial setting time

The early period in the hydration and strengthening of cement is referred as "initial setting" of cement. The initial setting time was measured by taking 50 g of HAC80 mixed with the percentage of water required for the normal consistency. In Vicat's apparatus a needle is allowed to penetrate through the cement block prepared. In the initial stage, a thicker needle is allowed to pierce through the test block. This procedure is repeated until the paste starts losing its plasticity, and the penetration is limited only to 5–7 mm depth. This duration of setting was counted and termed as the initial setting time.

2.4.3. Final setting time

The cement will be considered final set when, upon, falling the final setting plunger gently covers the surface of the test block and the needle makes no impression. The duration up to this process is considered as the final setting time.

HAC80 powder calcined at 1000 °C was analyzed for their microstructure at different magnifications with the help of FEI Quanta 200F field emission scanning electron microscope. Cold crushing strength (CCS) and three point bending strength (CMOR) of HAC80 as well as CA-25 C cement blocks cured

at 20 °C for 24 h, dried at 105 °C for 24 h and fired at 1000 °C for 3 h were determined according to ASTM C133-97.

2.5. Cordierite powder characterization

Powder X-ray diffraction patterns of calcined cordierite powder were recorded using a Rigaku portable high resolution powder X-ray diffractometer employing Cu $K\alpha_1$ radiation and Ni-filter. Data were collected in the 2θ range from 5° to 70°. Particle size distribution was done via Tyler sieve analysis, where prepared cordierite powder was separated on sieves of different sizes. It was then expressed as a range analysis, in which the percent amount of particles in each size range was listed in order.

2.6. Castable formulation

Low cement refractory castables were formulated using 5 wt % of prepared high alumina cement in the mechanochemically synthesized cordierite. As an additive two sources of silicon carbide viz. granular and whisker was added in a fixed 10 wt% of the mix. Castables with granular reinforcements were termed CSG whereas the ones containing whiskers were termed as CSW. Castables generally consist of precision graded coarse and fine refractory grains but in the present case only fine graded cordierite material prepared was used in the formulation. The trials of aggregate proportions were taken in a 1000 cm^3 flask filled up to 250 cm^3 and vibrated for 30 s. Packing density calculations were carried out for each trial. Aggregates having higher packing densities were chosen for further analysis. In the first step for cement castable matrix formulation, this castable pre-mix was dry mixed in a plastic container for 10 min with spatula. Generally, ultra and low cement castables require less than 5 wt% of water to achieve the desired rheology; therefore, water was added in two steps. The casting was done by adding the first two-thirds proportion of water at a time. Then, one-third of water was added slowly to get a homogeneous mixing. The wet mixing was performed up to 5–6 min to achieve proper flow. Immediately after doing wet mixing, the castable mix was filled into a rectangular and cubic shape mold of hard steel to prepare sample according to ASTM standards for cold modulus of rupture and cold crushing strength measurements respectively. The mold was placed on the vibrating table filled with the wet mixed castable and the mixes were vibrated for 10 min for enhanced compactness. For each composition, at least five samples were prepared for laboratory test. The samples were cured in a moisture saturated environment (95% RH) in a humidity chamber at room temperature for different time periods. Before firing the samples, they were oven dried at 110 °C for 24 h. The test samples were sintered at 1250–1400 ± 5 °C in an electric furnace with a dwell time of 3 h and at a heating rate of 5 °C/min.

2.7. Castable characterizations

Powder X-ray diffraction patterns of CSG and CSW series castables sintered at 1250–1400 °C were recorded using a Rigaku portable high resolution powder X-ray diffractometer employing Cu $K\alpha_1$ radiation and Ni-filter. Apparent porosity (A.P.) and bulk density (B.D.) were determined according to ASTM C20-00 [28] which involves boiling water bath. Cold crushing strength (CCS) and three point bending strength tests (CMOR) were done according to ASTM C133-97 [29] for a varying range of temperature (1250–1400 °C). Cyclic thermal stability of the refractories was determined experimentally by water quench test; ASTM C1171-05 [30]. Samples fired at 1350 °C were chosen for thermal shock analysis, as they

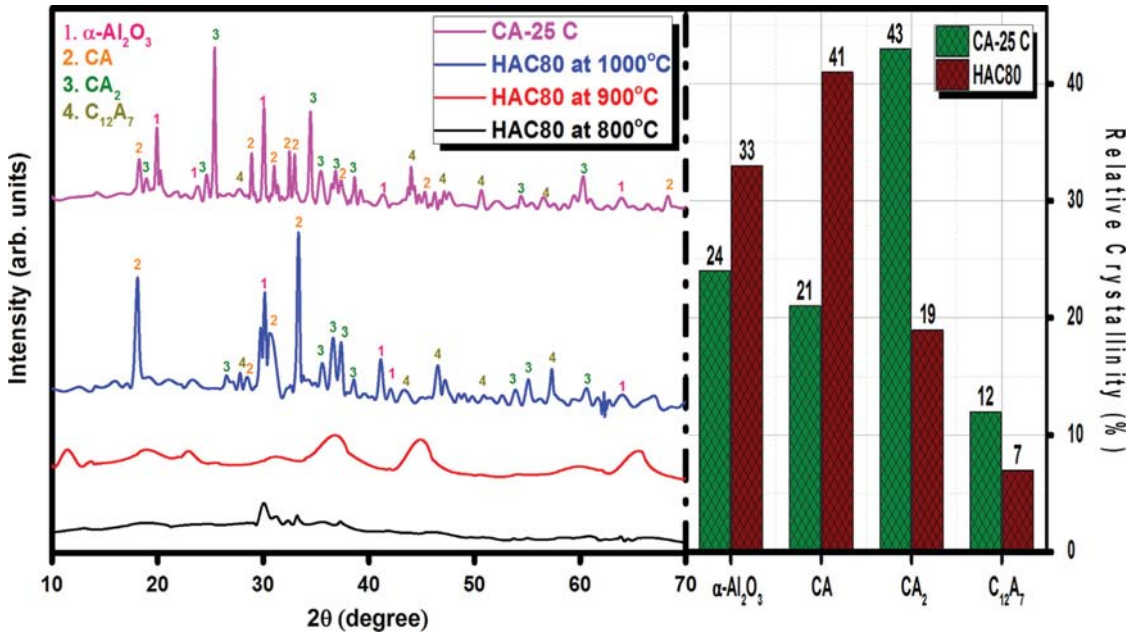

Fig. 1. HAC80 XRD pattern.

displayed superior crushing and bending strengths. The strength loss is measured by the difference in CMOR and CCS between un-cycled specimens and the specimens subjected to thermal cycling. This effect was evaluated as percentage deflection in residual CCS and residual CMOR after each cycle up to five such consecutive firings at 1000 °C and then subsequent water quenching at 25 °C for 20 min. This firing was done in an electric furnace containing SiC heating elements. These samples were also analyzed by SEM for their surface topology.

3. Results and discussion

3.1. Evolution of HAC80 phases by X-ray diffraction

Fig. 1 corresponds to the XRD patterns of samples of HAC80, calcined in the range 800–1000 °C. When calcined below 900 °C, these powders proved to have X-ray pseudo-amorphous pattern, whereas initial formation of calcium–aluminate phases may be envisaged. Pure crystalline cementing phases have just begun to form at 900 °C. A major improvement in crystallinity is evident when this cement sample was fired at 1000 °C. Prime phases investigated were CA, CA_2, and $C_{12}A_7$. These are readily formed and thermodynamically most stable compounds in the $CaO–Al_2O_3$ binary system [2,3]. These peaks were identified by standard JCPDS numbered 41-0358, 34-0440, and 09-0413 for their corresponding peaks of hexagonal CA, monoclinic CA_2, and cubic $C_{12}A_7$, respectively. Minor peaks of rhombohedral α-Al_2O_3 were also identified and matched with JCPDS 89-3072. In the conventional preparation route by high-temperature solid-state synthesis, the batch usually contains CaO-rich phases and unreacted Al_2O_3 before the appearance of desired product phase. The formation sequence of phases in these mixtures was always from calcia-rich phases to the alumina rich phase which could be accounted for the formation of $C_{12}A_7$. This was an interesting result because the soaking period in this process was as low as 10 min resulting in the energy saving process. The presence of broad peaks in XRD patterns of calcined cement powders shows that particle size is small. Crystallite size, d, of calcined powder was calculated from X-ray line broadening analysis using Scherrer's formula

$$d = \frac{0.9\lambda}{\beta \cos \theta} \tag{5}$$

where β is the full width at half maximum intensity of a Bragg reflection excluding instrumental broadening, λ is the wavelength of the X-ray radiation and θ is Bragg's angle. β is taken for the strongest Bragg's peak corresponding to 2θ. Crystallite size was evaluated to be 20 nm.

Relative crystallinity of the individual phases present was calculated with the help of commercially available software Origin 8.5. This assumption is based on the theory that relative crystallinity is the ratio between the sums of the plotted area of desired phase versus the total scattered plot area of all phases present.

$$\text{Relative crystallinity (\%)} = \frac{\sum(I\beta)\text{desired phase}}{\sum(I\beta)\text{all phases}} \times 100 \tag{6}$$

where I is the peak intensity and β is the full width at half maximum. Calculations indicate a 41 mass% formation of CA phase in HAC80 whereas only 21 mass% of CA was formed in CA-25 C. Other phase contributions were recorded to be 33 mass% (α-Al_2O_3), 19 mass% (CA_2), and 7 mass% ($C_{12}A_7$) of total HAC80 synthesized.

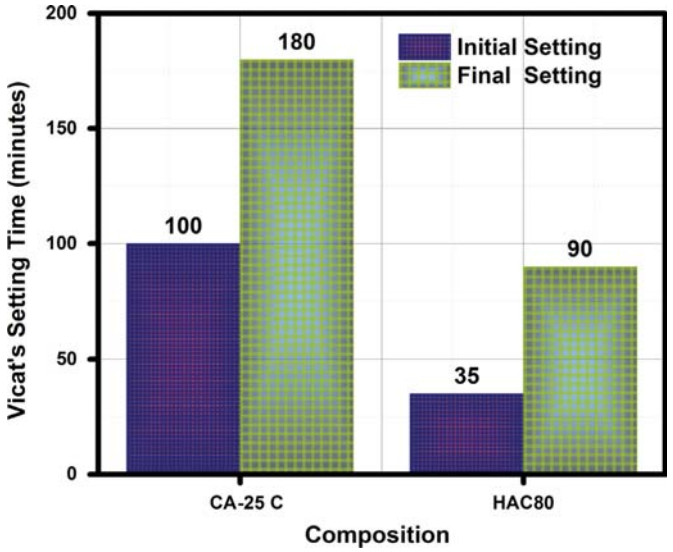

Fig. 2. Setting behavior of HAC80.

3.2. Setting behavior of HAC80

Fig. 2 shows the setting behavior of commercial and prepared high alumina cement. At room temperature, HAC80 had an initial setting time of 35 min and a final setting time of 90 min. The hydration behavior can be evinced when cement particles come into contact with water, they start to react yielding Ca^{2+} and $Al(OH)_4^-$ ions, leading to an increase of the pH and the ionic strength of the aqueous medium. After a certain period of time, the dissolved species achieve a supersaturation level in the aqueous solution, which persists until nuclei of calcium aluminate hydrates are formed. The nucleated hydrates are then rapidly grown, causing a marked decrease in the concentration of Ca^{2+} and $Al(OH)_4^-$ ions in the liquid medium [31]. Ample formation of CA crystalline phase (41 mass%) in HAC80 as when compared to 21 mass% of CA phase formed in CA-25 C decreased overall setting time. It is a well-known fact that reaction with water and formation of hydrate phases generally propagate from calcia rich phase to alumina rich phase. It is interesting that absence of ferrite phases and any alkaline impurity makes the cement more reactive which could also be the reason behind quick setting durations as compared to the standard CA-25 C.

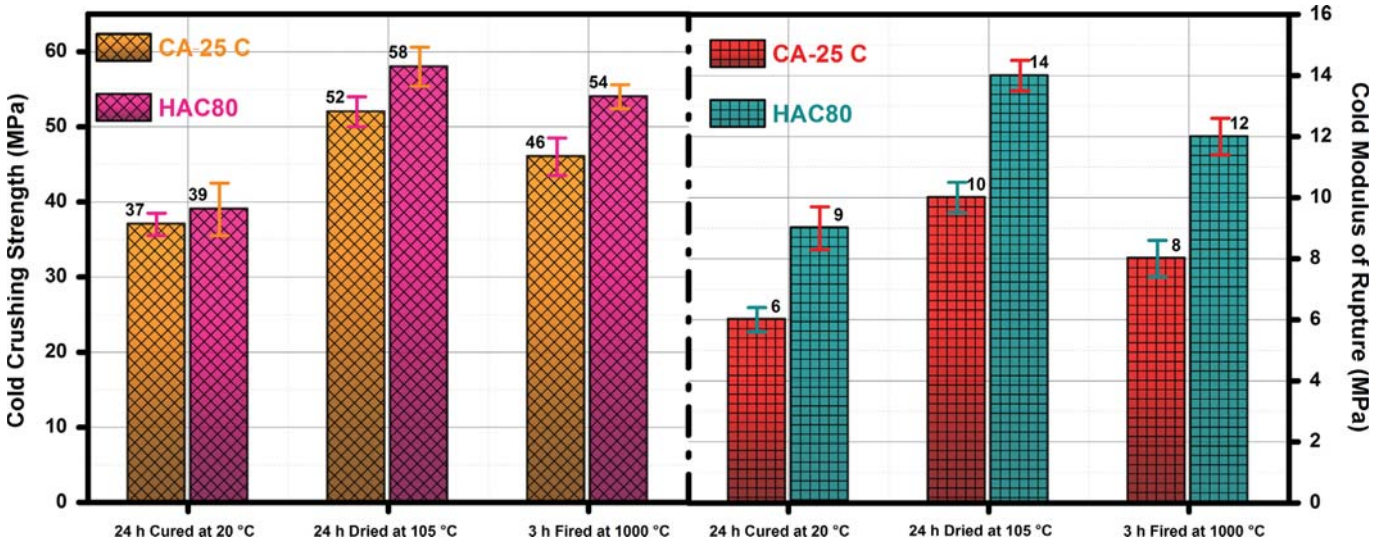

Fig. 3. CCS and CMOR of HAC80.

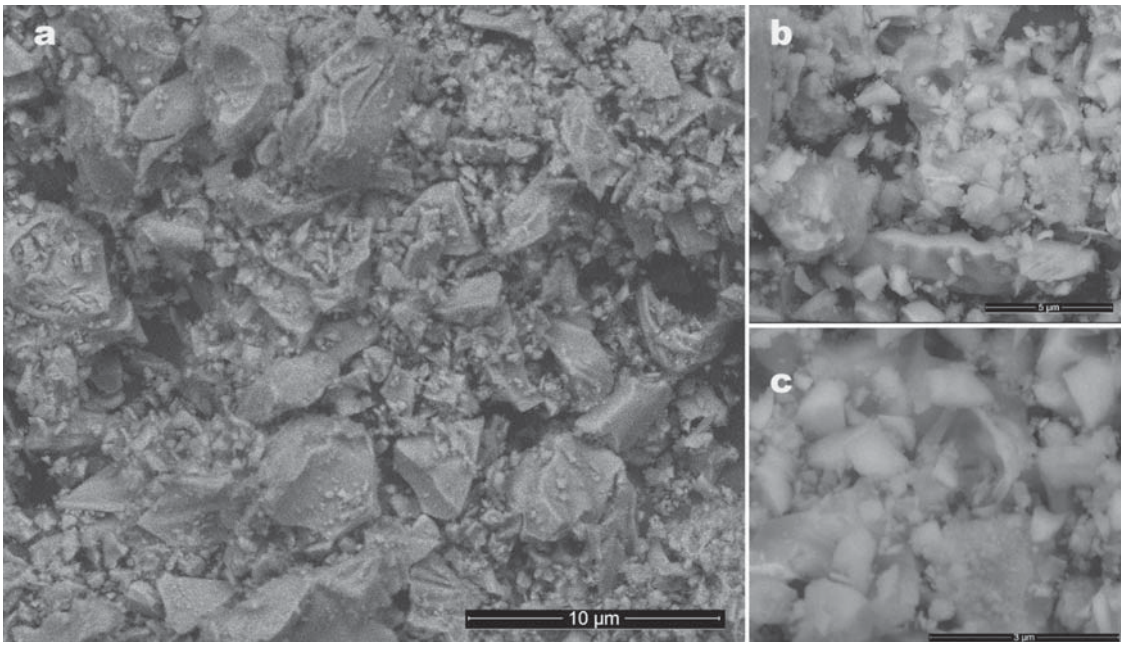

Fig. 4. HAC80 SEM.

3.3. CCS of HAC80 fired at 1000 °C

The pure (without any aggregates) HAC attained good structural strength as obtained from experimental procedure and shown in Fig. 3. It was observed that the strength increased rapidly with curing in both cements samples. The maximum CCS value obtained for HAC80 was 39 MPa. After drying at 105 °C for 24 h, it reached up 58 MPa and after 3 h firing at 1000 °C, it was obtained as 54 MPa. These results were better as compared to the samples prepared with commercially available CA-25 C cement. Samples attained its maximum strength after 24 h curing and subsequent 24 h dries. After this period there is a very slight variation. This reduction in strength is ascribed to the abrupt ending of incomplete hydration reaction. One more possible explanation to this could be an incomplete dehydration process. This process breaks the hydraulic bond and produces a drop of the mechanical resistance between 800 and 1200 °C. The higher strength of HAC80 is accredited to the presence of larger amounts of CA and CA_2. It is well known that CA and $C_{12}A_7$ react significantly in the early ages of hydration, and the hydration of $C_{12}A_7$ is very exothermic, so the formation of stable hydrates generally occurs sooner [6]. Although CA_2 is known to react slowly with water in the early stages of hydration, its presence along with other phases results in an overall faster hydration rate. The heat of hydration resulting

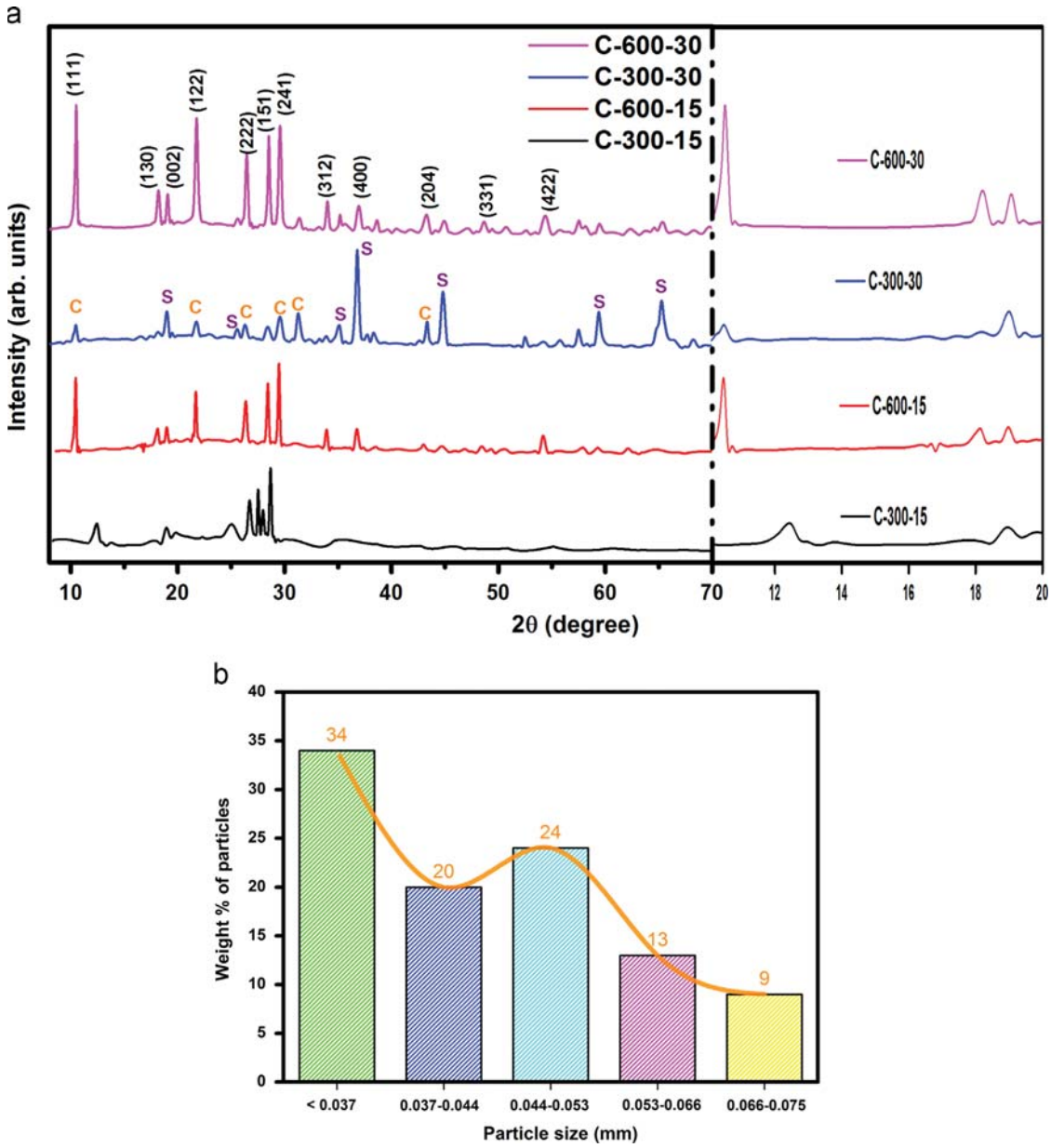

Fig. 5. (a) XRD pattern of prepared cordierite 1250 °C. (b) Cordierite particle size distribution.

from the hydration of CA activates CA_2 and makes it react relatively faster with water than it would do alone, but less than $C_{12}A_7$. After firing, the higher mechanical strength of HAC80 comparing with that of CA-25 C is due to the formation of a stable ceramic bond and the absence of any impure phase (alkaline compounds) owing to the purity of starting materials.

3.4. SEM of HAC80

Fig. 4 displays SEM photomicrographs of well-crystallized interlocking hexagonal plates of a CA matrix of HAC80 powder fired at 1000 °C. In this figure a, b and c signify different magnifications of the same sample. Some large features can be observed in addition to the homogeneous distribution of cement matrix. These features have not been analyzed by micro-analytical methods, but it is considered that they indicate the formation of CA as this was the most prominent phase calculated through XRD patterns. Isolated monoclinic phases of CA_2 and the dense clusters of cubic $C_{12}A_7$ plates are well distinct in all figures. The higher amount of CA and CA_2 is proposed to enhance the refractory properties. $C_{12}A_7$ phase is responsible for high bonding and quick hydration.

3.5. XRD pattern of prepared cordierite, formulated castables and its particle size distribution

Fig. 5(a) shows the XRD plot of prepared cordierite nanopowders calcined at 1250 °C. Two primary factors directly

determine the crystalline size of the samples, namely, nucleation and crystal growth processes. Sample coded as C-300-15 represents cordierite precursor milled at 300 rpm for 15 min and similar notifications were implemented for rest three samples. C-300-15 does not show any sign of cordierite and spinel formation. C-300-30 shows that μ-cordierite starts to form, but still major phase is recognized as a magnesium aluminate spinel ($MgAl_2O_4$). Spinel occurs as an intermediate phase which ultimately reacts with μ-cordierite at high temperatures to produce α-cordierite; α-cordierite itself is formed at temperatures $>1200\,^{\circ}C$. C-600-15 displays some crystalline phase appearance of α-cordierite which is better than C-300-30 sample in respect of cordierite formation. C-600-30 demonstrates complete phase crystallization of α-cordierite. Here extended figure again illustrates the complete formation of cordierite in C-600-30 samples. When comparing it with other three samples and focusing on a specific range, intense and sharp peaks corresponding to α-cordierite formation {110} plane at $2\theta=10.5^{\circ}$ are clearly depicted. In C-600-30 sample, {241} plane at $2\theta=29.5^{\circ}$ clearly demonstrated that improvement in crystallinity of cordierite is due to rise in milling speed and milling time. Cordierite peaks were matched with JCPDS data card 76-1794 and spinel peaks were identified by JCPDS data card 77-1193. XRD pattern of C-600-30 cordierite powder revealed a crystallite size of 35 nm. It can be well established that between two milling parameters, rotation speed is more effective than milling time. According, to these XRD pattern analysis C-600-30 was chosen for further studies for formulating castables.

Fig. 5(b) is a representation of particle size analysis done with the help of standard Tyler sieves 400, 325, 270, 250 and 200 mesh. Particles passing or remaining on certain sieves were tested for best particle packing density as explained in Section 2.7. It is an important parameter which has an effect on physical and chemical properties of briquettes prepared. It affects the strength, load-bearing properties and reactivity of solids participating in high temperature ceramic bond forming reactions. The use of particle packing principles provides the basis of the development of castable with low porosity, means for achieving high compaction in castable. Nature of ultra-fine particles decides the high temperature properties like creep behavior, corrosion resistance and hot strength.

Figs. 6 and 7 demonstrate the XRD patterns of cordierite castables with granular silicon carbide addition (CSG) and cordierite castables with whisker silicon carbide addition (CSW) respectively. Both were sintered at varying temperatures ranging from 1250 to 1400 °C. These two figures are almost similar expect few additional peaks of μ-cordierite in the CSG series castables are observed. Initially at lower temperature silicon carbide portrayed more prominent crystalline peaks, but when the temperature was raised above 1350 °C, its peak intensity started diminishing. This phenomenon could be in accordance with glassy phase appearance and excessive oxidation behavior of silicon carbide materials.

Sharp crystalline peaks of this low cement castables prepared, were identified and matched with JCPDS data card

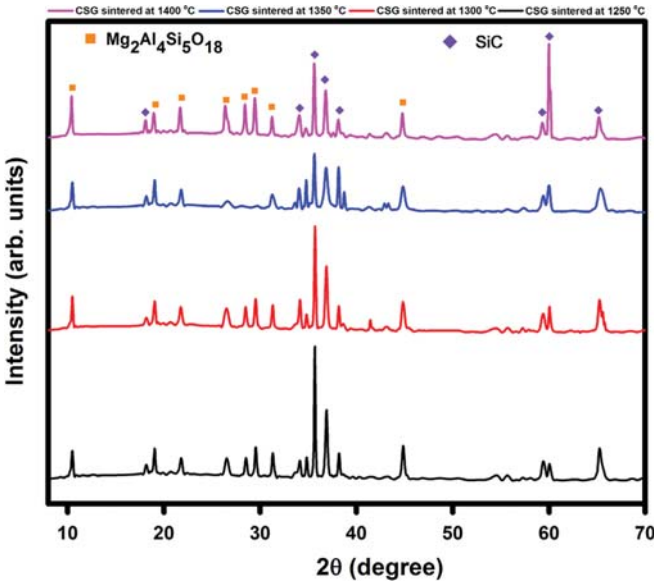

Fig. 6. XRD pattern of CSG castables.

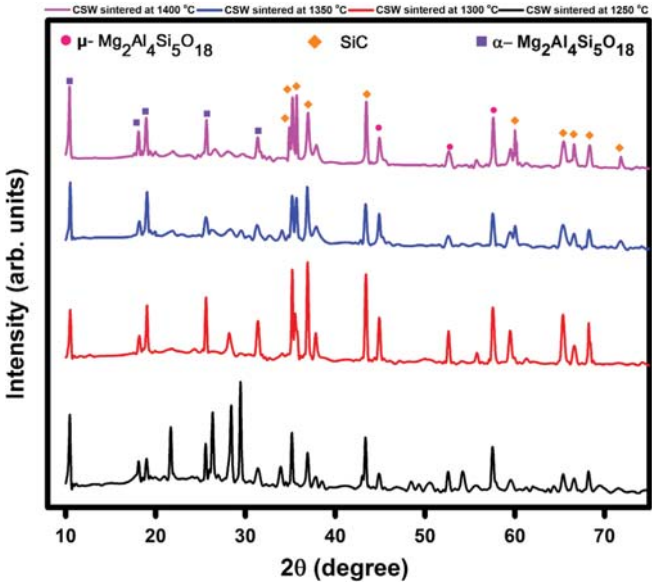

Fig. 7. XRD pattern of CSW castables.

65-0461 and 76-1794 for cordierite peaks and 89-4793 for α-silicon carbide peaks respectively. More of indialite (α-cordierite) peaks appeared in contrast to evanescing μ-cordierite peaks due to increase in sintering temperature.

3.6. Bulk density and apparent porosity of castables

Fig. 8 depicts the apparent porosity and bulk density of both series of castables sintered at varying temperature range. Although both formulations show similar results, whisker reinforcement has higher densities than granular reinforcements. The observed porosity of these materials may be explained by sintering theory. According to this theory, the densification and subsequent shrinkage of a compacted powder are achieved by the transport of material from the contact area

between grains through a thin liquid film to the off-contact neck region in final state sintering. This process results in a continuous reduction in pore size and a continuous change in grain shape that should become increasingly anhedral until the pore is completely eliminated [32]. An increasing trend in densities can be seen up to 1350 °C and after which it decreased a bit due to the excessive oxidation behavior of reinforced silicon carbide. Similarly porosities have a decreasing trend and they have slightly increased after the 1350 °C temperature is reached.

3.7. CCS, CMOR and thermal shock damage resistance of castables

Figs. 9 and 10 illustrate the temperature dependency and effect of consecutive residual thermal shock cycle on CCS and CMOR measurements. The curves representing CCS and CMOR have steep slopes in the initial stage, indicating an outstanding improvement proceeding rapidly with respect to sintering temperatures. The potential advantages of fibrous (whisker) additives over spherical (granular) reinforcement include more effective crack deflection and superior load-carrying capacity, which is quite evident from the modulus of rupture values. Other possible toughening mechanisms may include crack bridging and pullout. In Fig. 10 strengthening of castables with whisker reinforcement is attributed to the load transfer to the whisker. The stress distribution in a test bar subjected to a bending moment is such that a whisker is lying at right angles to the crack plane at the point of fracture, the maximum bending stress in the whisker will occur in the crack plane [21,33]. The sudden drop in mechanical strength with increasing temperature (> 1350 °C) is subjected to excessive oxidation of silicon carbide and in turn increasing content of oxidation derived silica melt. This phenomenon was similarly observed in the pure cordierite containing castables, which is expected because of the appearance of cordierite glass formation.

Present crushing and bending strength also draw an analogy to apparent porosity values which shows the maximum attained strength when a substantial decrease in porosity at 1300 °C is observed. After each cyclic thermal shock, a little decrement in residual CCS and CMOR value was observed. Samples subsequently retained a constant strength even after five such consecutive cycles. Thermal shock damage is more evident in residual bending strengths determined in CSW castable. Although bars representing residual crushing strength values do not show much alteration between CSW and CSG castable. The nature of the curve of the whisker reinforced cordierite castable is similar with a slight incrementing damage after thermal shock cycles. This may be correlated to the mean free path, which was greater in granular reinforced cordierite than that of the whisker reinforcement because of the larger dimensions of later phase. Improvement in mechanical strengths of these brittle ceramic is very important if these

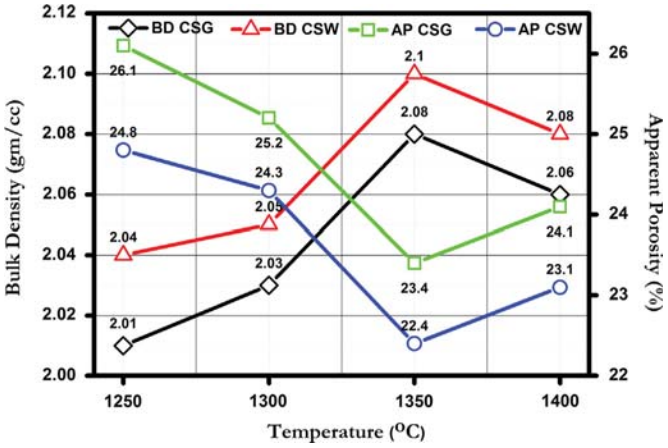

Fig. 8. AP BD of CSG, CSW.

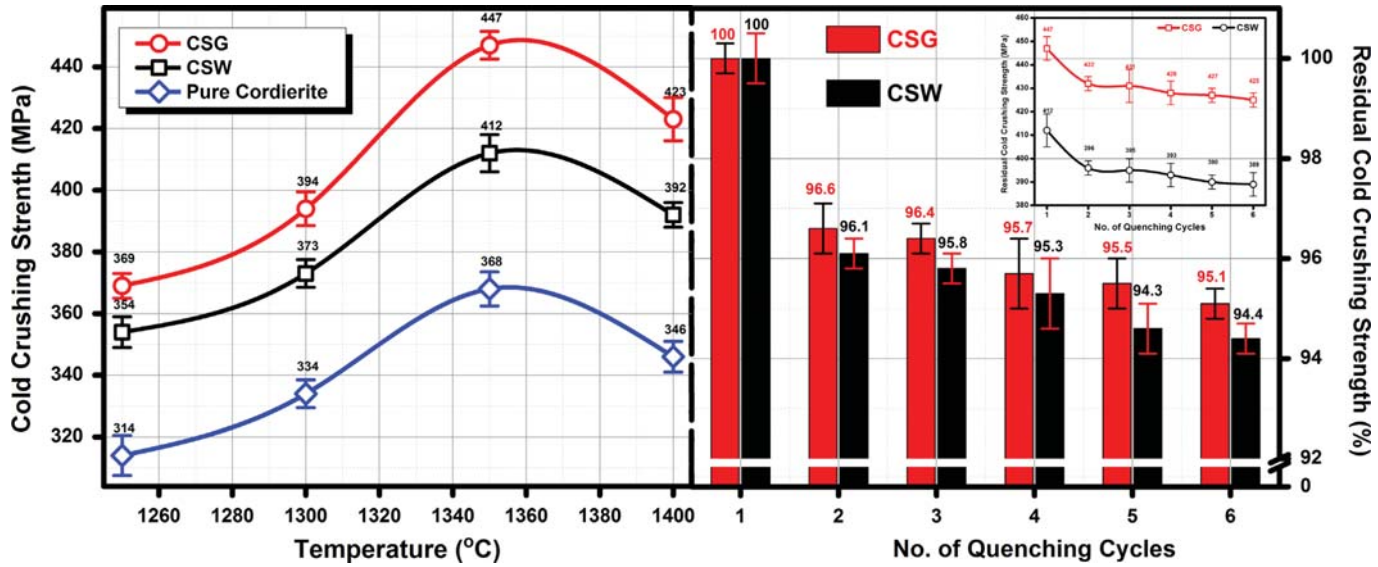

Fig. 9. CCS and cyclic CCS of CSG, CSW.

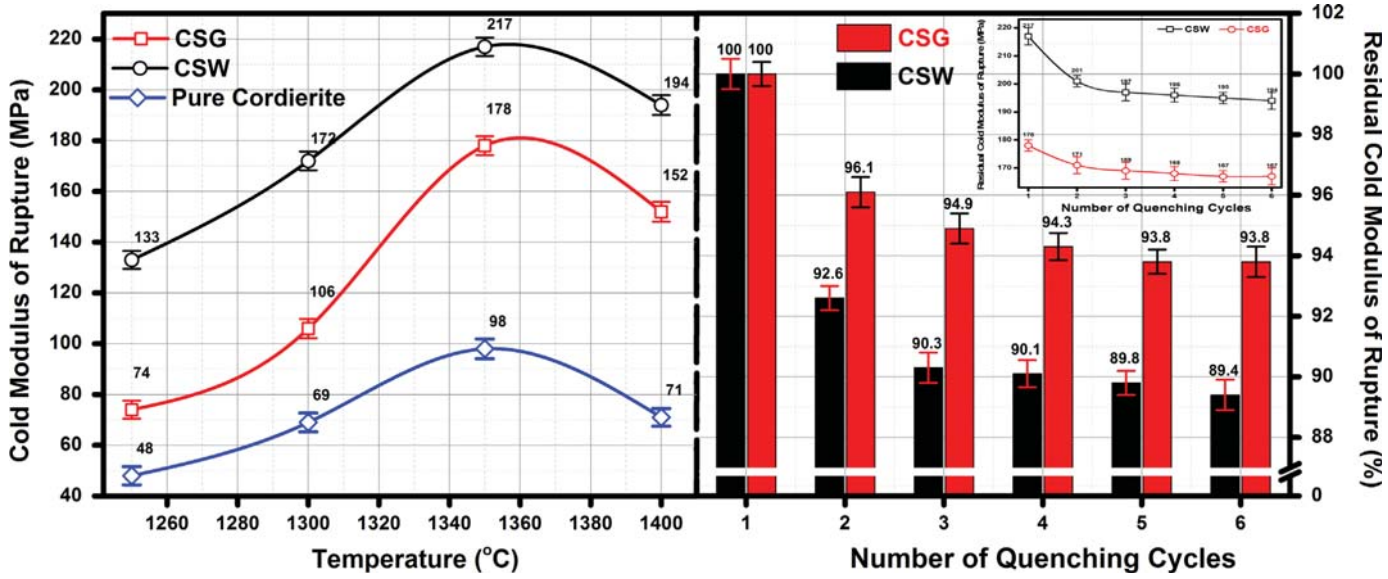

Fig. 10. CMOR and cyclic CMOR of CSG, CSW.

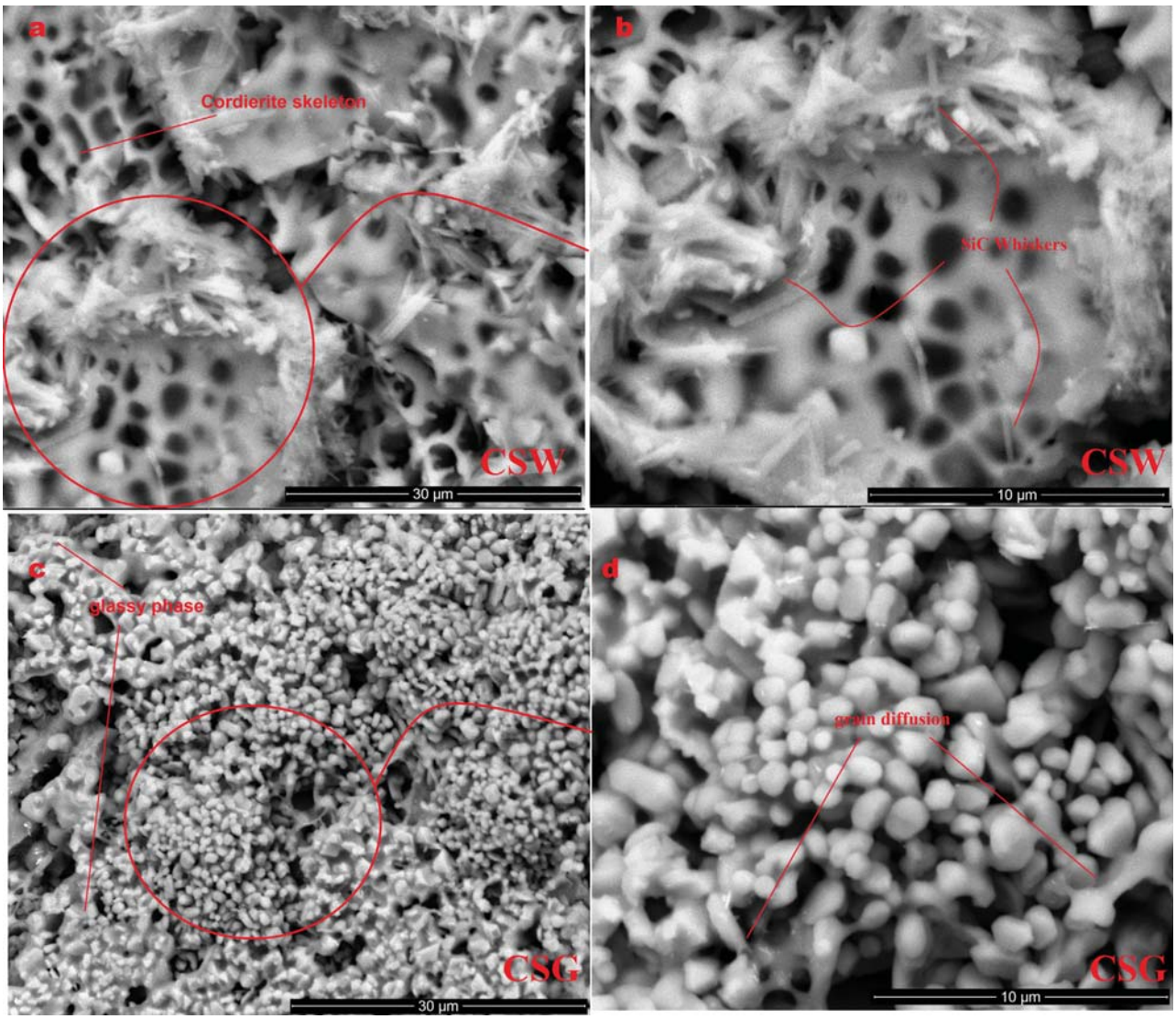

Fig. 11. SEM of CSW and CSG.

materials are to be used for load-bearing applications such as kiln furniture. Obtained results indicated that both materials are excellent candidates for the application where thermal shock resistance is required.

3.8. SEM of CSW and CSG castables sintered at 1350 °C

The microstructural growth of fractured specimens of castables fired at 1350 °C was examined using scanning electron microscopy. Fig. 11(a and b) depicts SEM photo-micrographs of CSW castable whereas Fig. 11(c and d) represents same of CSG castables. Only castables sintered at 1350 °C were chosen for analysis, as they represented superior thermo-mechanical and physical properties than all other castables sintered in low temperature ranges. Rod like shape is quite evident in CSW series while CSG depicted granular shapes. In Fig. 11(a and b), the well-developed bonding necks are formed between SiC particles and cordierite matrix. The influence of shaped ceramics precursor is well known and exploited in the control of densification, grain growth, and morphology during sintering. In Fig. 11(c and d), a coarse glassy single-phased grain can be seen, showing a high degree of reaction with a significantly lower matrix density. The bonding neck in CSG is thicker than whisker added castable CSW. This could be due to excessive oxidation of silicon carbide and subsequent formation of glassy silica. No evidence for whisker pullout was observed in this system under the test conditions used. In order for pullout to occur, the whiskers must first debond from the matrix and then be drawn from their sockets against frictional forces. At few points process of grain size growth occurrence can be seen, neck boundary diffusion between certain pores is observed as well as rounding of closed pores is observed.

4. Conclusions

1. Nanostructured high alumina cement with superior cementing properties than their commercialized equivalents was synthesized successfully through the auto combustion method.
2. Literature suggest that cordierite formation is always incorporated by magnesium–aluminate spinel phase. Hence, the addition of a sintering aid is essential to enhance complete phase formation of cordierite but this also reduces thermal shock in the final product. Here, mechanically activated precursors were successfully employed through optimized milling parameters to synthesize spinel free cordierite.
3. Silicon carbide acted as a reinforcing agent and its addition as whisker was found to help in improvement of bulk densities and in turn diminution of apparent porosities as compared with granular reinforcements.
4. The present study also revealed a relationship of the compressive strength as well as the flexural strength of prepared castables as a function of temperature. The obtained values of crushing and bending strengths in mechanochemically synthesized fine grained cordierite based castables prepared by using auto combustion processed high alumina cement are in good agreements with reported values. However there is a gradual deterioration of both the properties with increasing sintering temperature above 1350 °C but still it seems better than previously reported values.
5. The liquid phase formation due to the incongruent melting point of cordierite and excessive oxidation of silicon carbide at high temperature inhibit their uses for structural applications above 1400 °C. It is worth emphasizing that the presented results are consistent and is confirmed through numerous repeat of the measurement.

Acknowledgments

The authors gratefully acknowledge the financial support of DST [(TDT Division), Reference no. DST/SSTP/UP/197(G) 2012], Ministry of Science & Technology, New Delhi, India.

References

[1] Refractories Handbook, The Technical Association of Refractories, Tokyo, Japan, 1998.
[2] V. Kumar, V.K. Singh, A. Srivastava, G.N. Agrawal, Low temperature synthesis of high alumina cements by gel-trapped co-precipitation process and their implementation as castables, J. Am. Ceram. Soc. 95 (12) (2009) 3739–3775.
[3] V. Kumar, V.K. Singh, A. Srivastava, Low temperature synthesis of high alumina cements by novel Co-melt precursors and their implementation as castables with some micro fine additives, J. Am. Ceram. Soc. 96 (7) (2013) 2124–2131.
[4] A. Srivastava, V.K. Singh, V. Kumar, P.H. Kumar, H. Tripathi, A. Chaudhary, K. Asiwal, R. Pandey, S.K. Suman, Some studies on ceria–zirconia reinforced solvothermally synthesized cordierite nano-composites, J. Alloys Compd. 586 (2014) 581–587.
[5] J.B. Rodrigues, R. Moreno, Rheological behavior of kaolin/talc/alumina suspensions for manufacturing cordierite foams, Appl. Clay Sci. 37 (2007) 157–166.
[6] D.A. Fumo, M.R. Morelli, A.M. Segadaes, Combustion synthesis of calcium aluminates, Mater. Res. Bull. 31 (1996) 1243–1255.
[7] R. Ianos, I. Lazau, P. Cornelia, P. Barvinschi, Fuel mixture approach for solution combustion synthesis of $Ca_3Al_2O_6$ powders, Cem. Concr. Res. 39 (2009) 566–572.
[8] C.L. Aguilar, M.A. Aghayan, M.A. Rodrıguez, Solution combustion synthesis and sintering behavior of $CaAl_2O_4$, Ceram. Int. 38 (2012) 395–399.
[9] N. Sakhare, S. Lunge, S. Rayalu, S. Bakardjiva, J. Subrt, S. Devotta, N. Labhsetwar, Defluoridation of water using calcium aluminate material, Chem. Eng. J. 203 (2012) 406–414.
[10] A. Zapata, P. Bosch, Low temperature preparation of belitic cement clinker, J. Eur. Ceram. Soc. 29 (2009) 1879–1885.
[11] M. Hirano, H. Inada, Preparation and characterization of cordierite–zirconia composites from co-precipitated powder, J. Mater. Sci. 28 (1993) 74–78.
[12] N.T. Andrianov, S.R. Abdel, N.V. Zenkova, Synthesis and sintering of cordierite sol–gel powders based on different magnesium salts, Glass Ceram. 63 (2006) 6–9.
[13] C.S. Hong, et al., Synthesis and sintering of amorphous cordierite powders by a combustion method, J. Mater. Sci. Lett. 13 (1994) 1361–1363.
[14] S. Zhu, S. Ding, H. Xi, Q. Li, R. Wang, Preparation and characterization of SiC/cordierite, composite porous ceramics, Ceram. Int. 33 (2007) 115–118.
[15] M. Dimitrijevic, M. Posarac, J. Majstorovic, T. Volkov-Husovic a, B. Matovic, Behavior of silicon carbide/cordierite composite material after cyclic thermal shock, Ceram. Int. 35 (2009) 1077–1081.

[16] M.A. Camerucci, G. Urretavizcaya, A.L. Cavalieri, Sintering of cordierite based materials, Ceram. Int. 29 (2003) 159–168.
[17] S. Liu, Yu-ping Zenga, D. Jiang, Effects of CeO_2 addition on the properties of cordierite-bonded porous SiC ceramics, J. Eur. Ceram. Soc. 29 (2009) 1795–1802.
[18] B. Fotoohi, S. Blackburn, Effects of mechanochemical processing and doping of functional oxides on phase development in synthesis of cordierite, J. Eur. Ceram. Soc. 32 (2012) 2267–2272.
[19] K.P. Gadkaree, Whisker reinforcement of glass-ceramics, J. Mater. Sci. 26 (1991) 4845–4854.
[20] Z. Acimovic, L. Pavlovic, L. Trumbulovic, L. Andric, M. Stamatovic, Synthesis and characterization of the cordierite ceramics from nonstandard raw materials for application in foundry, Mater. Lett. 57 (2003) 2651–2656.
[21] I. Wadsworth, R. Stevens, Strengthening and toughening of cordierite by the addition of silicon carbide whiskers, platelets and particles, J. Mater. Sci. 26 (1991) 6800–6808.
[22] S. Li, Y. Zhang, J. Han, Y. Zhou, Zirconia reinforced reaction bonded silicon carbide composites: Microstructure and mechanical properties, Int. J. Refract. Met. Hard Mater. 35 (2012) 257–261.
[23] W. Chi, D. Jiang, Z. Huang, S. Tan, Sintering behavior of porous SiC ceramics, Ceram. Int. 30 (2004) 869–874.
[24] A. Yamuna, R. Johnson, Y.R. Mahajan, M. Lalithambika, Kaolin-based cordierite for pollution control, J. Eur. Ceram. Soc. 24 (2004) 65–73.
[25] J. She, T. Ohji, Z.-Y. Deng, Thermal shock behavior of porous silicon carbide ceramics, J. Am. Ceram. Soc. 85 (2002) 2125–2127.
[26] M. Posarac, M. Dimitrijevic, T. Volkov-Husovic, A. Devecerski, B. Matovic, Determination of thermal shock resistance of silicon carbide/cordierite composite material using nondestructive test methods, J. Eur. Ceram. Soc. 28 (2008) 1275–1278.
[27] IS: 4031-4, Method of physical tests for hydraulic cement, Part 4 Determination of consistency of standard cement paste (first revision), 1988, pp. 1–6.
[28] ASTM C20-00, Standard Test Methods for Apparent Porosity, Water Absorption, Apparent Specific Gravity, and Bulk Density of Burned Refractory Brick and Shapes by Boiling Water. 2010.
[29] ASTM C133 − 97 (Reapproved 2008) Standard Test Methods for Cold Crushing Strength and Modulus of Rupture of Refractories.
[30] ASTM C1171 − 05 (Reapproved 2011) Standard Test Method for Quantitatively Measuring the Effect of Thermal Shock and Thermal Cycling on Refractories.
[31] A.R. Studart, M.D.M. Innocentini, I.R. Oliveira, V.C. Pandolfelli, Reaction of aluminum powder with water in cement-containing refractory castables, J. Eur. Ceram. Soc. 25 (2005) 3135–3143.
[32] D.-H. Vu, K.-S. Wang, B.X. Nam, B.H. Bac, T.-C. Chu, Preparation of humidity-controlling porous ceramics from volcanic ash and waste glass, Ceram. Int. 37 (2011) 2845–2853.
[33] H. Suzuki, K. Ota, H. Saito, Mechanical properties of alkoxy-derived cordierite ceramics, J. Mater. Sci. 23 (1988) 1534–1538.

Journal of Alloys and Compounds 586 (2014) 581–587

Contents lists available at ScienceDirect

Journal of Alloys and Compounds

journal homepage: www.elsevier.com/locate/jalcom

Some studies on ceria–zirconia reinforced solvothermally synthesized cordierite nano-composites

Abhinav Srivastava *, Vinay Kumar Singh, Vijay Kumar, P. Hemanth Kumar, Himanshu Tripathi, Ashish Chaudhary, Krit Asiwal, Rahul Pandey, Shyam Kumar Suman

Department of Ceramic Engineering, Indian Institute of Technology (BHU), Varanasi, India

ARTICLE INFO

Article history:
Received 13 August 2013
Received in revised form 12 September 2013
Accepted 20 September 2013
Available online 1 October 2013

Keywords:
X-ray diffraction
Scanning electron microscopy
Solvothermal process
Nano-composites

ABSTRACT

Nanostructured cordierite and 12 mol% ceria stabilized zirconia were chemically prepared separately. Pure cordierite was synthesized solvothermally, whereas $[(Zr)_{0.88}(Ce)_{0.12}O_2]$ termed as CeSZ was processed with gelation and co-precipitation method. The evolution of crystalline phases and the microstructures have been studied using X-ray diffractometer, and FE-SEM with EDX. Varying contents (0–20 weight%) of CeSZ were then mixed with cordierite to form sample blocks of desired shapes. These nano-composite blocks were fired at 1100–1400 °C for a soaking time of 3 h to observe their thermo-mechanical, micro-structural and physical properties. Results indicate that ceria not only acts as a stabilizer in zirconia ceramics but it also acts as a sintering aid in cordierite formation. CeO_2 also improves compressibility and structural properties of nano-composites. Sintering temperature also plays an important role in the behavior of nano-composite blocks. All properties show a major improvement than previous reported data's.

1. Introduction

In recent years, nano-crystalline ceramics and the application of nano particles to improve the ceramic properties have attracted considerable interest, as the mechanical, optical, electrical and magnetic properties are crystallite size sensitive. Natural cordierite ($Mg_2Al_4Si_5O_{18}$) is a rare magnesium–alumino-silicate mineral occurring in nature [1–3]. The cordierite ceramics are known due to their low thermal expansion coefficient, high chemical durability, low dielectric constants, high refractoriness and excellent resistance to thermal shock. However, cordierite ceramics are susceptible to low fracture toughness, which hinders their structural applications. Unfortunately processing of synthetic cordierite is difficult as it is always accompanied by a spinel ($MgAl_2O_4$) phase, which impairs the thermal shock resistance of end product due to its high thermal expansion coefficient. It is difficult to produce dense cordierite ceramics by the solid-state reaction without sintering aids because of the narrow sintering range near the incongruent melting point of cordierite [4,5].

Ceria stabilized tetragonal zirconia (CeSZ) polycrystalline ceramics possess distinct advantages over other conventional structural ceramic materials because of their better thermal stability in moist environments, wider range of solid solubility in tetragonal region [6]. Consequently, ceria stabilized zirconia ceramics have been investigated extensively for structural applications. The grain size and microstructure of these materials are difficult to control in conventional technique. Gelation and co-precipitation process is a promising candidate for production of CeSZ particles giving a better control over size and shape of the synthesized nano-powders [7,8].

There is some data available on the cordierite synthesis by the novel chemical processes but not for structural properties [9]. The aim of this study was the synthesis of nanostructured cordierite by solvothermal technique and investigation of the phase transformation during heat treatment of precipitate. Addition of ZrO_2 (mostly in tetragonal form) in cordierite has been extensively studied but very little is known about its cubic polymorph reinforcement with effect of mineralizer additions on both the sinterability and the mechanical properties of cordierite bodies fabricated by wet chemical routes. The effect of CeO_2 as mineralizer has been studied in the present work with the addition of cubic ZrO_2 in nanostructured cordierite matrix. To do this CeSZ was incorporated in thus prepared cordierite matrix and blocks were formed to investigate their micro-structural and mechanical properties.

2. Materials and methods

2.1. Synthesis of nanostructured cordierite by solvothermal technique

A solvothermal process [10–12] was used to synthesize the cordierite nano-powders. All reagents were analytical grade, purchased from LobaChem (Mumbai, India) and used as received. First appropriate metal-nitrate precursors; $Mg(NO_3)_2 \cdot 6H_2O$, $Al(NO_3)_3 \cdot 9H_2O$ and orthosilicic acid (H_4SiO_4) were dissolved in deionized

* Corresponding author. Tel.: +91 9454730609.
E-mail address: srivasabhinav@gmail.com (A. Srivastava).

0925-8388/$ - see front matter © 2013 Elsevier B.V. All rights reserved.
http://dx.doi.org/10.1016/j.jallcom.2013.09.150

water–ethanol (1:1 volume ratio) under rigorous stirring to form 0.5 molar solution. The precursors were taken in a ratio to give a stoichiometric composition of cordierite. To this solution 100 g of urea and 1 mmol sodium dodecyl sulfate (SDS) was subsequently added. The solution was sealed in a tightly closed stainless steel autoclave and heated at 120 °C for 12 h. Upon completion of the reaction, the product was centrifuged at 10,000 rpm for 5 min and washed with deionized water and ethanol. The resulting precipitate was dried at 100 °C for 24 h and then calcined at varying range of temperature (1100–1300) °C for a soaking period of 2 h to obtain cordierite nano-powders.

2.2. Synthesis of $[(Zr)_{0.88}(Ce)_{0.12}O_2]$ by gelation and co-precipitation method

AR grade $ZrOCl_2{\cdot}8H_2O$ and $Ce(SO_4)_2{\cdot}4H_2O$ were dissolved in deionized water with vigorous stirring and mild heating to give 12 mol% ceria stabilized zirconia $[(Zr)_{0.88}(Ce)_{0.12}O_2]$. For preparation of gel, ammonia solution was added drop wise and pH of the solution was maintained over 9. A point was reached when the gel became fully viscous and the process of stirring was stopped due to the viscous nature of the gel. This gel was oven dried at 100 °C for 24 h and finally calcined at 750 °C for 5 h to give super fine CeSZ [13–15].

2.3. Preparation of nano-composites

Batches were formed employing above processed nano-powders of cordierite and CeSZ in the varying ratio. Nanostructured cordierite formed at 1300 °C was selected for the formulation of nano-composites as by the X-ray diffraction analysis it showed the lowest content of spinel phase and highest content of α-cordierite. A zero weight% CeSZ containing cordierite mix was named CZ00. Similarly 5, 10, 15 and 20 weight% CeSZ containing cordierite mixes were named CZ05, CZ10, CZ15 and CZ20 respectively. These batches were pulverized in a high energy planetary ball mill. The jar and grinding media were of titanium-coated stainless steel material. At one time 250 g of a batch was taken in a jar and milled for 45 each min at 600 rpm. Similarly, it was processed to complete the grinding of all batches. These nano-powdered batches were then cold pressed into desired blocks as per ASTM standards by a uniaxial hydraulic press machine under a constant 10 tones pressure load. Several blocks of each composition were made and sintered in a temperature range of 1100–1400 °C for a soaking period of 3 h. Sintered and dense composite blocks were investigated for their thermo-mechanical and micro-structural properties [16,17].

2.4. Characterization of the nano-composites

Powder X-ray diffraction patterns were recorded using a Rigaku high resolution powder X-ray diffractometer employing Cu $K\alpha_1$ radiation and Ni-filter. Data were collected in the 2θ range from 0° to 90°.

Synthesized and sintered blocks of formulated composites were examined using a FEI Quanta 200F Field Emission Scanning Electron Microscope (FE-SEM). The samples were metalized by gold sputtering for better image definition.

Apparent Porosity and Bulk Density of sintered nano-composite were investigated according to ASTM C20-00.

The Cold Crushing Strength (CCS) is the capacity of a material to withstand axially directed pushing forces. Cubic test specimens of 51 mm size were prepared and the value of maximum uniaxial load (in N) was noted when the sample block failed completely. Finally CCS value was calculated using the method stated in ASTM C133-97.

Cold modulus of rupture (CMOR) measurements was carried out under three-point bending tests (ASTM C133-97) using 152 mm × 25 mm × 25 mm samples.

Sample briquettes were measured for their mechanical strength in terms of cold crushing strength (MPa) and modulus of rupture (MPa) according to ASTM C133-97.

3. Results and discussions

Fig. 1 shows the XRD plot of as prepared cordierite nano-powders. Two primary factors directly determine the crystalline size of the samples, namely, nucleation and crystal growth processes. At lower temperature 1100 °C the μ-cordierite starts to form but still the major phase is recognized as a magnesium aluminate spinel ($MgAl_2O_4$). Spinel occurs as an intermediate phase which ultimately reacts with μ-cordierite at high temperatures to produce α-cordierite; α-cordierite itself is formed at temperatures >1200 °C. Here inset figure illustrates the complete formation of cordierite focusing on a specific range which clearly depicts intense and sharp peaks corresponding to α-cordierite formation {1 1 0} plane at $2\theta = 10.5°$. In sample calcined at 1200 °C {2 4 1} plane at $2\theta = 29.5°$ portray improvement in crystallinity of cordierite due to rise in synthesis temperature. Cordierite peaks were matched

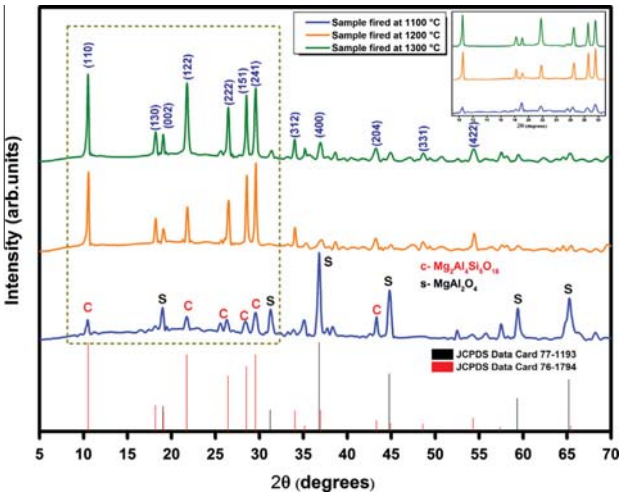

Fig. 1. XRD plot of solvothermally prepared cordierite.

with JCPDS data card 76-1794 and spinel peaks were identified with JCPDS data card 77-1193.

Presence of broad peaks in XRD patterns of calcined powders show that particle size is small. Crystallite size, d of calcined powder was calculated from X-ray line broadening analysis using Scherrer's formula.

$$d = 0.9\lambda/\beta\mathrm{Cos}\theta$$

where β is the full width at half maximum (FWHM) intensity of a Bragg reflection excluding instrumental broadening, λ is the wavelength of the X-ray radiation and θ is the Bragg angle. β is taken for the strongest Bragg's peak corresponding to 2θ. All the three cordierite powders calcined have an average crystallite size in the range 20–35 nm.

Fig. 2 reveals the formation of gelation and co-precipitation processed 12 mol% ceria stabilized zirconia. No evidence of crystalline impurities is found in the pattern. Cubic ZrO_2 peaks matched exactly with JCPDS data card 65-0461. These results indicate that the cubic ZrO_2 with high phase-purity can be obtained in the process reported. In addition, according to the Scherrer's formula, the average crystallite size of the sample is evaluated to be approximately 18 nm from the half-peak width of the {1 1 1} diffraction peak at $2\theta = 30.13°$.

Particle size distribution of as prepared Cordierite and CeSZ is shown in Fig. 3. IJ1.46 tool was used to identify and count the number of particles as well as their mean diameters. Maximum

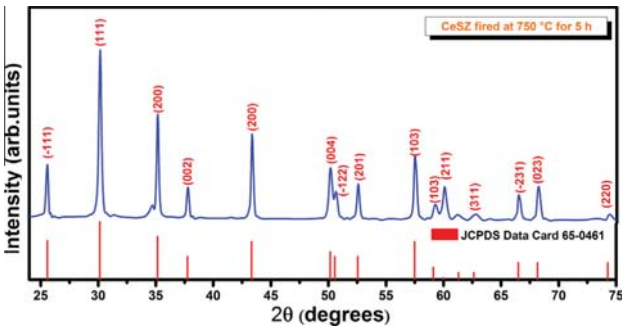

Fig. 2. XRD plot of gelation and co-precipitation processed 12 mol% ceria stabilized zirconia.

Cordierite particles lay in the range 0.02–0.06 μ and for CesZ it was dispersed from 0.01 to 0.08.

The examination of the fabricated cordierite-zirconia, nanocomposite by Fig. 4 enabled us to identify the component-phases formed after sintering, which shows an overall improvement in crystalline behavior of zirconia peaks. This can be related to the increasing content of stabilized zirconia and relatively increasing content of ceria. In contrast to previous works of similar compositions [2,7,9] where mullite and zircon diffraction peaks appeared as one of the major phases of final sintered samples, in present study none of them are detected, this could be attributed to the ceria addition, giving stabilization through formation of cubic cerium zirconium oxide.

As expected ceria not only stabilized zirconia but also improved the crystalline nature of α-cordierite peaks, suppressing any residual phase formation. Sharp crystalline peaks of composite were identified and matched with JCPDS data card 65-0461 and 76-1794. More of indialite (α-cordierite) peaks appeared in contrast to evanescing μ-cordierite peaks due to increase in cubic ceria–zirconia content. Ceria acts as a dissolution agent for magnesium-aluminate spinel ($MgAl_2O_4$) and its peaks vanished when CeSZ content was increased.

In Fig. 5 the theoretical density, bulk density and apparent porosity is portrayed. Variations of the density of the obtained materials depend on the amount of CeSZ in the green body as well as the selected level of sintering temperature which is apparently illustrated in the figure. It is worth noting that the present data are consistent with these demonstrated by Hirvonen et al. [3] for cordierite/ZrO_2 composite which indicates that composite density systematically increases with the content of zirconia in the sintered body.

Dual representation in Figs. 6 and 7 which is representation of thermo-mechanical behavior of the composites prepared provides a better understanding of thermal as well as compositional changes occurring. The curves representing CCS and Cold MOR have similar shapes and are regularly spaced. These curves have steep slopes in the initial stage, indicating an outstanding improvement proceeding rapidly with respect to sintering temperatures. Both the properties cold crushing strength and modulus of rupture have an increasing trend with increase in the CeSZ content. Sintering temperature has a positive effect in densification and strengthening behavior up to 1300 °C after which it decreases. Here again, however the attainable strengths at highest temperature is not satisfactory but a maximum service temperature can be reckoned. This sudden drop in mechanical strength with increasing temperature is

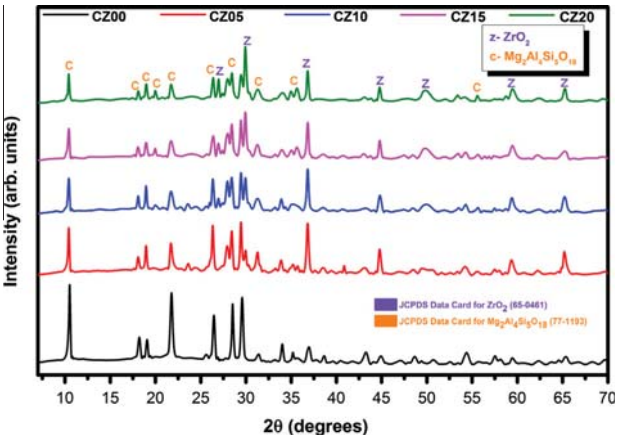

Fig. 4. XRD plot of composites prepared and fired at 1300 °C.

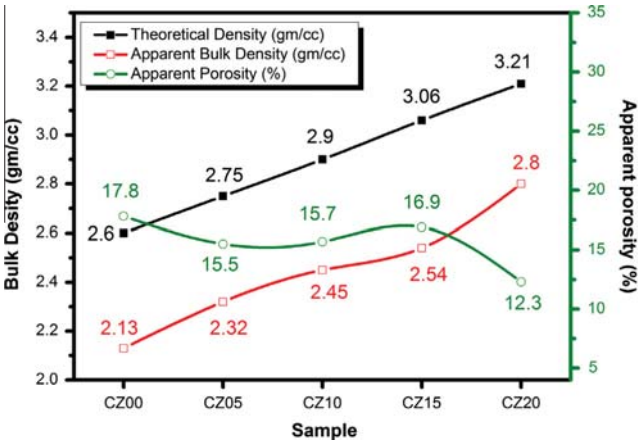

Fig. 5. Bulk density and apparent porosity of composite fired at 1300 °C.

subjected to increasing content of liquid content and appearance of amorphous phases. At 1400 °C an estimated 43 volume% liquid phase was formed [18].

Fig. 8 is the powder micrograph of as prepared cordierite and nanostructured cubic ceria doped zirconia which consists of very fine primary particles, approximately 18 nm in size. The irregular

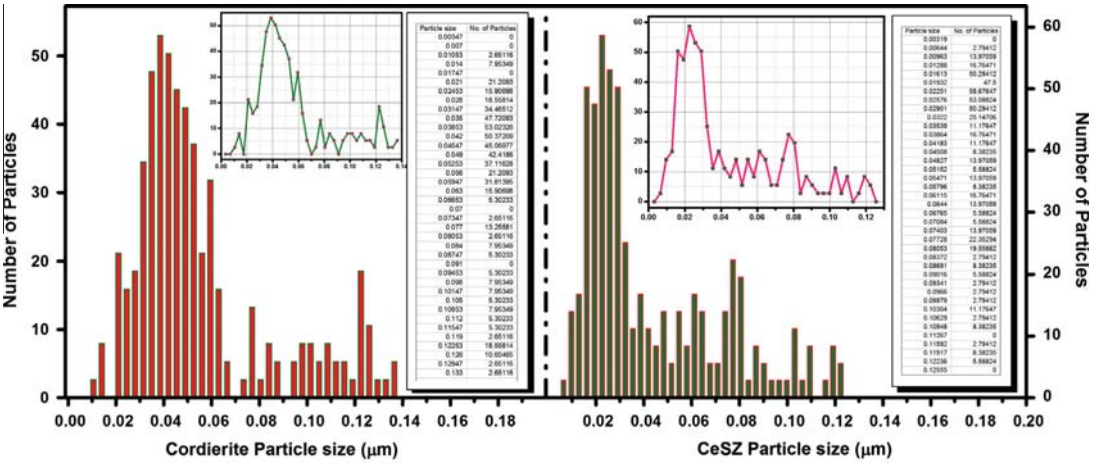

Fig. 3. Particle size distribution.

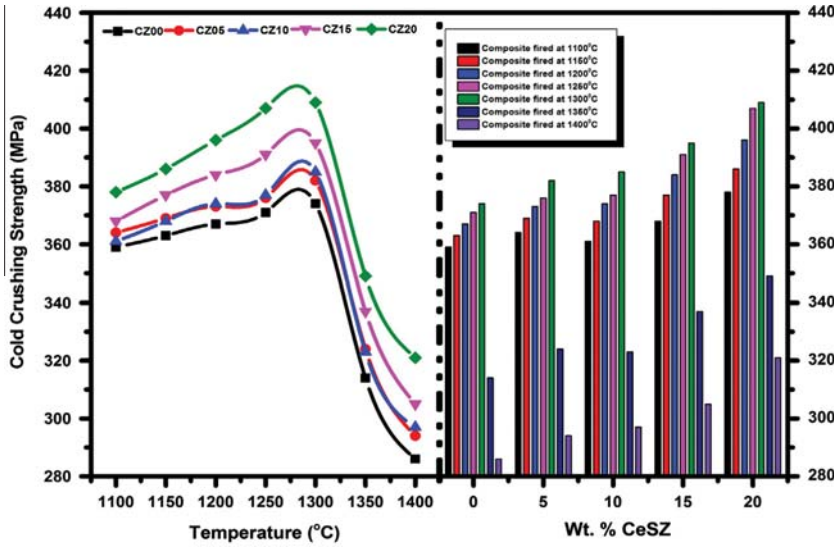

Fig. 6. Cold crushing strength of nano-composite fired at different temperatures.

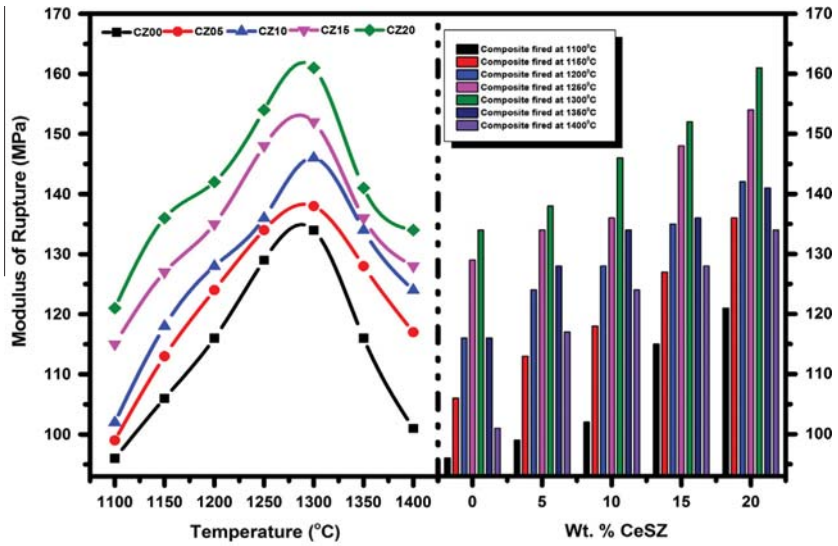

Fig. 7. Modulus of rupture of nano-composite fired at different temperatures.

bulky shapes can be predicted to be of ceria as it has larger ionic radii. Pure nano-crystalline α-cordierite called indialite (stable hexagonal form) in the micrograph shows an open microstructure. This open microstructure appearance is due to sample swelling during the phase change from μ to α without further densification with sintering temperature. EDS microanalysis shows that the calcined powder retained a near stoichiometric composition of cordierite.

Figs. 9 and 10 illustrate the structure of the obtained nano-composites observed using field emissive scanning electron microscopy of the fractured surfaces revealing sub-micron size grains of 5–20 weight% CeO_2–ZrO_2 accompanied by continuous predominant indialite glassy grain boundary phase. The morphology of the investigated material did not differed significantly with the applied sintering temperature, so only samples sintered at 1300 °C are shown here. The nano-size powder prepared by above mentioned wet chemical routes was very effective in improving densification. Cubic structured CeO_2–ZrO_2 particles can be observed homogeneously dispersed on the surface of cordierite matrix in Figs. 9 and 10. The black areas correspond to pores in the microstructure, which seems to be a result of the β to α modification of cordierite. Hexagonal grains with hint of pseudo-reticulated shape are seen in the all the composites due to the liquid phase sintering, this interlocking of crystalline grains could be termed responsible for such high mechanical strengths. Fig. 11 displays glassy indialite matrix in which small crystals of CeSZ can be envisaged. Significantly greater densification was observed when composition moved towards higher CeSZ addition. In samples CZ15 and CZ20 where ceria is added in relatively high volumes, the product becomes glassier in nature with the cerium oxide acting as a fluxing agent. Increasing content of zirconia and ceria can be clearly observed through the EDS pattern which also provides a complete compositional chart. In addition, the average composition calculated from three data points by EDS analysis showed that the powder had a uniform spatial distribution of constituent phase on a nano-size scale.

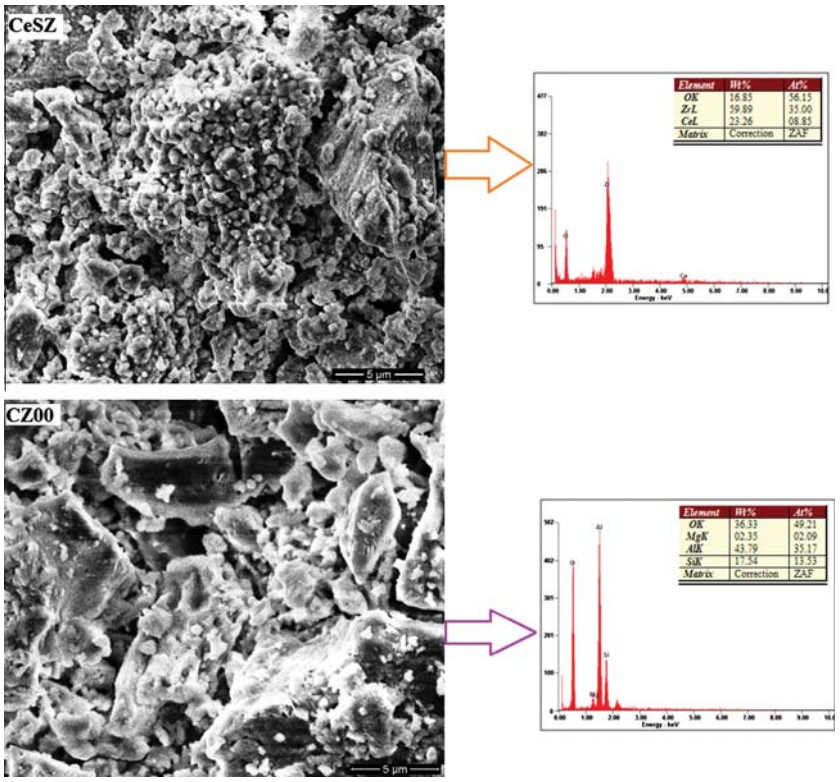

Fig. 8. FE-SEM and EDS plot of ceria stabilized zirconia and pure cordierite prepared.

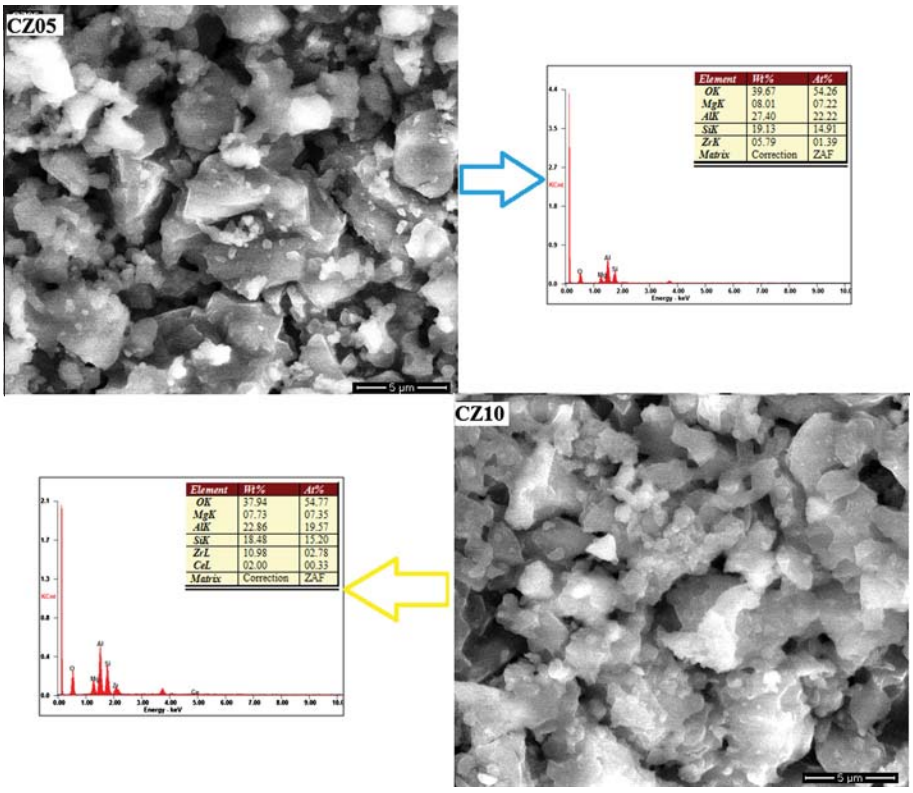

Fig. 9. FE-SEM and EDS plot of cordierite composite containing 5 and 10 weight% CeSZ.

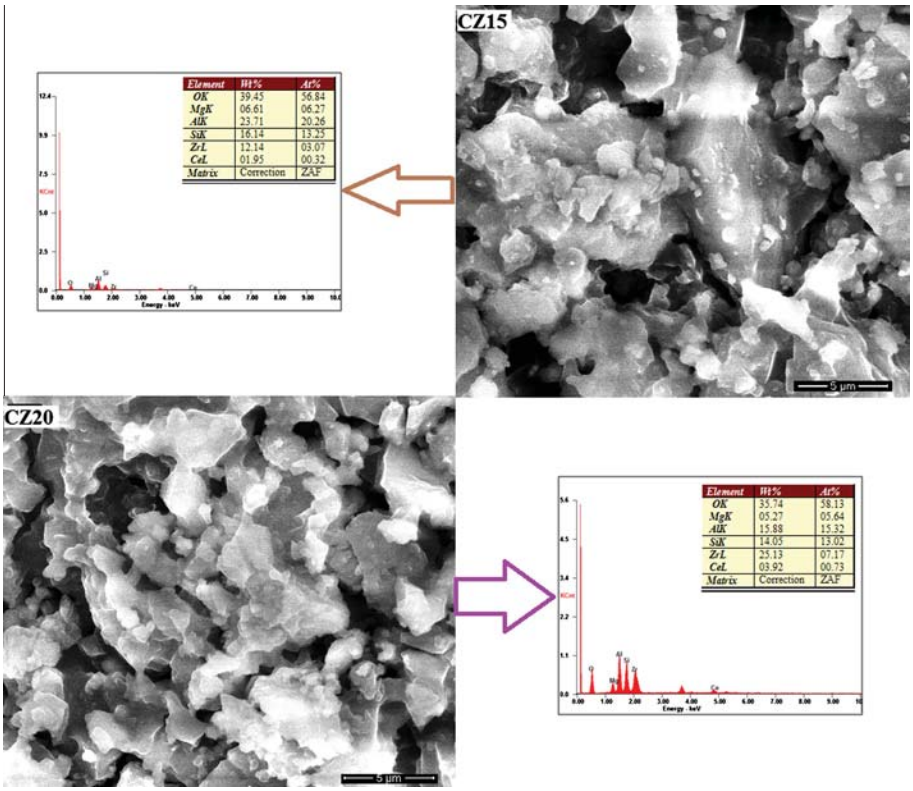

Fig. 10. FE-SEM and EDS plot of cordierite composite containing 15 and 20 weight% CeSZ.

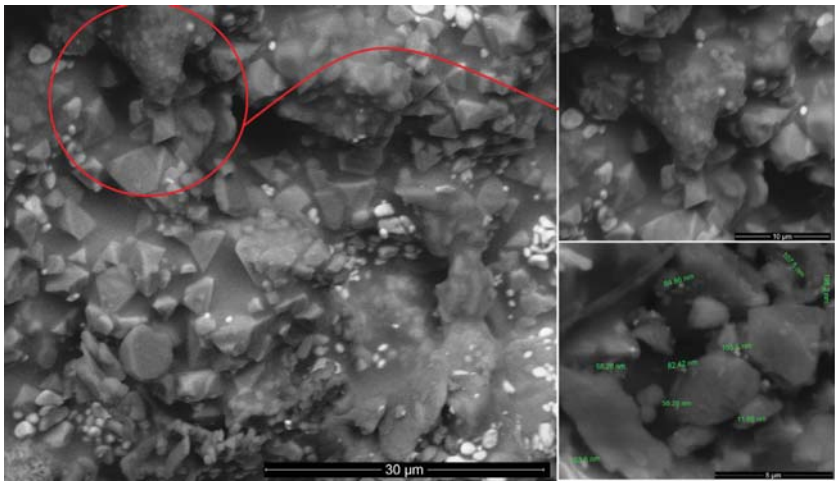

Fig. 11. CZ20 at 1300 C.

4. Conclusions

Nanostructured cordierite and CeSZ were synthesized successfully by two novel processing techniques. Literatures suggest that cordierite formation is always supported by a spinel phase and hence increasing calcinations temperature with addition of a sintering aid was done successfully to remove any residual phases. Ceria acts as a stabilizer in zirconia ceramics and it was found to help in improving crystallinity of α-cordierite formed by acting as a sintering aid. CeO_2 also improves compressibility of nanocomposites which is evident by the physical property measurements. The process limited the formation of zircon and mullite, apparently due to formation of stable cubic cerium zirconium oxide. It had been reported that making a dense cordierite body is very difficult as it has an open structure but present work succeeds in achieving bulk densities near to its theoretical density. The obtained mixture of two high-strength materials displays, however, interesting combination of mechanical properties coupled with desired physico-thermal stability.

The present study revealed that the compressive strength as well as the flexural strength of the obtained nano-composites depends on the weight percent of cubic ceria–zirconia present. Unfortunately, from the technological point of view, the observed gradual deterioration of both the properties with increasing sintering temperature above 1300 °C fails short from required characteristics but still it is far better than previous reported values. The

present authors claim that this drawback can be improved by proper selection of the fabrication conditions, since there are several toughening mechanisms available in zirconia system.

The liquid and amorphous phase formations at high temperature inhibit their uses for structural applications above 1400 °C. It is worth emphasis that the presented results are consistent, i.e., confirmed through numerous repeating of the measurement and the structural properties show a major improvement compared to previous reported values. The obtained material through novel processing routes appears to be an interesting candidate for thermal insulation, and its production involves the phenomena that need further clarification to be applied in a controlled manner.

Acknowledgments

The authors gratefully acknowledge the financial support of DST [(TDT Division), Reference No. DST/SSTP/UP/197(G) 2012], Ministry of Science & Technology, New Delhi, India. We gratefully acknowledge the valuable assistance of Mr. Bhagmal, Mr. Ashish Tripathi and Mr. Mansharam with the XRD, SEM and MOR measurements.

References

[1] Sang-Jin Lee, Waltraud.M. Kriven, Crystallization and densification of nano-size amorphous cordierite powder prepared by a PVA solution–polymerization route, J. Am. Ceram. Soc. 81 (1998) 2605–2612.
[2] En.-Hai. Sun, Takafumi Kusunose, Tohru Sekino, Koichi Niihara, Fabrication and characterization of cordierite/zircon composites by reaction sintering: formation mechanism of zircon, J. Am. Ceram. Soc. 85 (2002) 1430–1434.
[3] A. Hirvonen, R. Nowaka, Y. Yamamoto, T. Sekino, K. Niihara, Fabrication, structure, mechanical and thermal properties of zirconia-based ceramic nanocomposites, J. Eur. Ceram. Soc. 26 (2006) 1497–1505.
[4] S.Z. Mohamed Shamshuddin, M. Shyam Sundar, N. Thimmaraju, Venkatesh, G. Vatsalya, M. Senthilkumar, Synthesis, characterization and catalytic activity studies on cordierite honeycomb coated with ZrO_2 based solid super acids, C. R. Chim. 15 (2012) 799–807.
[5] Shuang Li, Yumin Zhang, Jiecai Han, Yufeng Zhou, Zirconia reinforced reaction bonded silicon carbide composites: microstructure and mechanical properties, Int. J. Refract. Met. Hard Mater. 2012 (35) (2012) 257–261.
[6] L. Li, O. Van Der Biest, P.L. Wang, J. Vleugels, W.W. Chen, S.G. Huang, Estimation of the phase diagram for the ZrO_2–Y_2O_3–CeO_2 system, J. Eur. Ceram. Soc. 21 (2001) 2903–2910.
[7] F.A. Costa Oliveiraa, J. Cruz Fernandes, Mechanical and thermal behaviour of cordierite–zirconia composites, Ceram. Int. 28 (2002) 79–91.
[8] Shifeng Liu, Yu-ping Zenga, Dongliang Jiang, Effects of CeO_2 addition on the properties of cordierite-bonded porous SiC ceramics, J. Eur. Ceram. Soc. 29 (2009) 1795–1802.
[9] V.S. Nagarajan, K.J. Rao, Preparation and thermal evolution of the microstructure of sol–gel-derived cordierite and cordierite–zirconia powders, J. Solid State Chem. 94 (1991) 149–162.
[10] M. Yoshimura, K. Byrappa, Hydrothermal processing of materials: past, present and future, J. Mater. Sci. 43 (2008) 2085–2103.
[11] Elvin Beach, Samantha Brown, Krenar Shqau, Matthew Mottern, Zack Warchol, Patricia Morris, Solvothermal synthesis of nanostructured NiO, ZnO and Co_3O_4 microspheres, Mater. Lett. 62 (2008) 1957–1960.
[12] Anukorn Phuruangrat, Titipun Thongtem, Somchai Thongtem, Novel combined sonochemical/solvothermal syntheses, characterization and optical properties of CdS nanorods, Powder. Technol. 233 (2013) 155–160.
[13] Vijay. Kumar, Vinay Kumar Singh, Abhinav Srivastava, Gokul Nath Agrawal, Low temperature synthesis of high alumina cements by gel-trapped co-precipitation process and their implementation as castables, J. Am. Ceram. Soc. 95 (2012) 3769–3775.
[14] Vinay Kumar Singh, B. Ravindra Reddy, Synthesis and characterization of bioactive zirconia toughened alumina doped with HAp and fluoride compounds, Ceram. Int. 38 (2012) 5333–5340.
[15] V.P. Singh, D. Das, Chandana Rath, Studies on intrinsic defects related to Zn vacancy in ZnO nanoparticles, Mater. Res. Bull. 48 (2013) 682–686.
[16] Z.M. Shia, Y. Liu, W.Y. Yang, K.M. Liang, F. Pan, S.R. Gu, Evaluation of cordierite–ceria composite ceramics with oxygen storage capacity, J. Eur. Ceram. Soc. 22 (2002) 1251–1256.
[17] Vijay Kumar, Vinay Kumar Singh, Abhinav Srivastava, Low temperature synthesis of high alumina cements by novel co-melt precursors and their implementation as castables with some micro fine additives, J. Am. Ceram. Soc. 96 (2013) 2124–2131.
[18] Refractories Handbook, The Technical Association of Refractories, Tokyo, Japan, 1998.

Issn 0973-9777 Volume-6 Number-2 March-April 2012

The Indian Journal of Research Anvikshiki

Bi-monthly International Journal of all Research
www.onlineijra.com

Engineering and Technology

MPASVO
MANEESHA Publications

Letter No.V-34564,Reg.533/2007-2008
ANVIKSHIKI ISSN 0973-9777

INDIAN JOURNAL OF RESEARCH(2012) **6,58-62**
Advance Access publication 16 Jan. 2012

A REVIEW ON THE IMPLEMENTATION OF HIGH CARBON BINDERS IN REFRACTORIES TECHNOLOGY

ABHINAV SRIVASTAVA*, VIJAY KUMAR and V. K. SINGH

Declaration

The Declaration of the authors for publication of Research Paper in The Indian Journal of Research Anvikshiki ISSN 0973-9777 Bi-monthly International Journal of all Research: We, *Abhinav Srivastava, Vijay Kumar and V. K. Singh* the authors of the research paper entitled A REVIEW ON THE IMPLEMENTATION OF HIGH CARBON BINDERS IN REFRACTORIES TECHNOLOGY declare that , We take the responsibility of the content and material of our paper as We ourself have written it and also have read the manuscript of our paper carefully. Also, We hereby give our consent to publish our paper in Anvikshiki journal , This research paper is our original work and no part of it or it's similar version is published or has been sent for publication anywhere else.We authorise the Editorial Board of the Journal to modify and edit the manuscript. We also give our consent to the Editor of Anvikshiki Journal to own the copyright of our research paper.

Abstract

The authors review the literature sources of various authors and foreign companies in the field of application of high-carbon organic binders for refractories, composites and technical ceramics. The review reveals the advantages of the new generation of binders with improved properties and describes binders meeting contemporary environmental requirements and not containing free phenol and other carcinogenic and toxic components.

Keywords: Carbon, Phenol, Binders, Refractories

Binders play a crucial role in production of refractories, fireproof composites, and corrosion-resistant ceramics (electrodes, vessels, pipes) in the Al - Mg - Ca - O - Si - C system. The expansion of the product range and the increase in the volume of refractory ceramic production are stimulating extensive development of efficient binders and their active implementation. Foreign manufacturers [1] center their attention on developing highly advanced and environmentally safe binders for refractories and engineering ceramics.

The nature of high-carbon binders, as well as fillers, is the most important factor affecting the quality of ceramic and refractory products. The binder undergoes deep physico-chemical modifications in the course of curing and firing, and nevertheless, unlike the traditional temporary technological binder, it remains a part of the end material (product or lining) in modified (coked) form. Approximately half of the binder is removed in firing, and fired samples contain 15 - 20% coked binder [2]. Organic binders with a high coke residue are the most valuable [2,3], since carbon diminishes penetration of slag and serves to increase the heat-resistance of the art [4]. Therefore, a high-carbon binder to a great extent predetermines the technical properties of a product, its

*(Corresponding Author) Department of Ceramic Engineering (Institute of Technology) Banaras Hindu University Varanasi (U.P.) India. e-Mail : srivasabhinav@gmail.com

manufacturing technology, and operating conditions. In this context, the homogeneity of composition and storage and transport stability of a binder are of special importance. Not all technologically efficient binders have a high coke residue.

The main requirements imposed on binders used in production of carbon-containing refractory materials and linings are the following:

- environmental safety
- High carbon content of the binder and substantial coke residue (at least 40%)
- storage stability
- good flow characteristics and adhesion to mineral filler particles providing a high degree of homogeneity during mixture preparation and molding
- Accessibility and reasonable price.

Until recently, the most common binder in production of dolomite and periclase products was coal pitch whose assets include a high content of residual coked carbon and a low price [2,9]. The cost of refractories based on a coal pitch binder is usually 10- 20% lower than those based on a synthetic binder.

However, the yield of coke residue cannot be the only criterion in selecting a binder. Indeed, coal pitch is a blend of indefinite chemical composition containing a substantial amount of polycyclic aromatic hydrocarbons of carcinogenic nature [7]. On thermal decomposition, pitch produces 1, 2-benzopyrene, benzoanthracene, perylene, alkylbrazan, etc. [10-12]. It is possible to reduce the benzopyrene content nearly to one-tenth using high-temperature treatment of refractories based on a pitch binder, but the substantial investments and power consumption required in that case offset the effect of the low cost of the products. The use of coal pitch necessarily implies coking firing that involves numerous manual labor operations in hard working conditions. Due to all of these factors, manufacturers of carbon ceramics and refractories have abandoned pitch-based binders.

The binders generally used in production of periclase articles are based on lignosulfonates obtained in the wood pulp and paper industry by refining of sulfite lye [13]. Lignosulfonates are high-molecular compounds consisting of aromatic nuclei linked by propane residues in non-polar chains with inclusions of polar carbonyl, carboxyl, sulfo and hydroxide groups. The presence of certain functional groups determines the specific properties of lignosulfonates [10,14]. Lignosulfonates exhibit high surface-active parameters, good binding capacity, and are sufficiently common products, although they have low coke residue and contain ammonium that is displaced in reaction with magnesium oxide, which is undesirable regarding environmental safety [14].

The concentrates of sulfite-alcohol distillery residues that were used in production of refractories prior to lignosulfonates are currently not produced by the domestic pulp and- paper industry, although they have better binding power than lignosulfonates.

A significant quality factor of carbon-containing products is their strength at temperatures above 1000^0C. At present, the materials predominantly used abroad are synthetic resins, above all, furan and phenol resins belonging to an extensive group of thermosetting synthetic resins: melamine, resorcin, carbamide, epoxy, unsaturated polyester, and other resins [15].

The common features of phenol formaldehyde and furan resins include a high degree of polymerization, three-dimensional structure of the carbon skeleton providing for heat resistance, high coke residue, possibility of application both in the liquid and the solid state, as well as lower power consumption than required in production of coal tar.

It is known that the reaction between phenol and formaldehyde depending on the conditions generates different varieties of phenol-formaldehyde resin: novolacs or resols. The former are solid compounds with a softening point of 70-110^0C the latter exist in the liquid or solid form with a softening point of up to 70^0C. In production of refractories abroad, both varieties are used in the following forms:

- Resin of novolac type in solid form or in solution

- Powder of novolac type resin mixed with urotropine
- Resin of resol type as aqueous solution or dissolved in another solvent.

Novolacs are meltable and soluble in organic solvents. They are supplied as lumps or granules when in solid form. Solvents most commonly used for phenol resins of the novolac type are univalent and multivalent alcohols and esters. When employing phenol solution as a binder, a curing agent is added at the end of the mixing process, such as uritropine (hexamethylene tetramine) or para-formaldehyde.

The addition of these compounds results in formation of cross links, curing starts at temperature of 110-120^{0}C where the curing rate is dependent on the temperature. Mixtures of phenol novolac with hexamethylene tetramine are distinguished by the fact that the latter is present in the powder from the beginning in the amount of 5 -15% and the same as the temperature, determines the resin curing rate [15].

Extensive use of phenol-formaldehyde resins (PFR) as binders in ceramic technology is due to the following facts:

- adhesion to both oxide and oxygen-free fillers and the good flow parameters of composites based on PFR
- curing of raw material at relatively low temperatures in a short time
- thermosetting of PFR (resin in a refractory batch is cured and partly pyrolyzed at about 350^{0}C therefore complete pyrolysis results in significant power savings in production of refractories)
- sufficient strength of lining based on phenol-formaldehyde resin
- heat resistance of refractory products based on PFR facilitated by the three-dimensional structure of the polymer formed after resin curing through poly-condensation of oligomers
- The strong carbon skeleton of PFR after heat treatment, with high residual carbon content, which determines the most significant service properties of refractories, i.e. resistance to slag and metal.
- Products based on phenol-formaldehyde binder do not undergo a clearly expressed plastic phase; therefore they keep their shape well.

Another advantage of phenol and furan resins is the increase in the strength of refractories in the course of resin carbonization due to their lattice structure [15]. This is a distinction of PFR from other carbon binders, such as coal pitch. PFR have relatively high coke residue, which is supported by thermo-gravimetric measurements [5,7]. However, PFR represent such a serious environmental threat that international and Russian environmental authorities call for the exclusion of PFR from production technologies. The most dangerous component of this binder is free phenol. Industry using phenol resins are noted for increased toxicity and the explosion hazard [10]. Nevertheless, replacement of PFR with an equally efficient binder is a difficult problem, since PFR surpasses many industrially produced polymers in physicochemical parameters and efficiency.

The free phenol content is of the utmost importance when selecting a phenol resin of the resol type. The resin previously used contained 20-25% free phenol, which did not meet the requirements of EU legislation specifying that the phenol content should not exceed 5%. In this connection, new resins meeting the required specifications were developed abroad.

German scientists developed a phenol resol characterized as an environmentally safe material with high adhesion to filler components, sufficient storage stability of the prepared mixture, and maximum strength after hardening and coking [3]. The authors note that the concentration of toxic substances in production can be reduced significantly if cold mixing technology is applied. By using phenol resol and thermal poly-condensation, one can do without urotropine and organic solvents. Moreover, this binder does not release benzo-pyrene in the course of decomposition.

Anhydrous phenol resins of the resol type developed by Bakelite GmbH (Germany) are widely used in production of non-fired refractories and fireproof composites. They do not contain polycyclic hydrocarbons, and their content of free phenol and formaldehyde is below 1% [16].

Powdered phenol resins and novolac resin solutions obtained according to advanced technologies practically do not contain free phenol and are considered to be environmentally safe [17]. However, the appearance of these resins on the market brought about certain modifications in the technology of non-fired products due to some

specific properties of the binders caused by the kinetics of their thermal decomposition. Application of the new type of binders requires reconstruction of production technology and using heating equipment designed for a temperature of 800^0C since thermal disintegration of these binders begins at temperatures above 300^0C and ends at 800^0C with release of the paraffin series compounds that form the polymeric carbon skeleton binding the matrix.

Furan resins are pure or mixed liquid polymers based on furfuryl alcohol (furfural). In thermosetting and binding capacities, this type of resin is close to phenol resins. In the process of resin curing at temperatures above 300^0C a three-dimensional carbon skeleton with a sufficiently high carbon residue is formed. The advantage of furan resins is that they are produced from vegetable materials, while phenol resins are based on products of oil and coal processing. Yet, in spite of that, furan resins did not receive wide acceptance in production of refractories abroad.

Foreign producers are developing binders based on resins containing no carcinogenic aromatic hydrocarbons and halogens. Another area for improving the environmental safety of refractory production is the development and implementation of organic binders containing absolutely no phenol. Application of such binders makes it possible to solve simultaneously the problem of increasing the hydration resistance of the product, improving the mixture moldability and in some cases increasing the operating characteristics of the product. The experience in industrial application of natural resins is widely known, but resins of that type used in the 60-70s contained aromatic heterocyclic compounds (benzene, toluene, xylene, phenol, cresol, benzopyrene, pyridine), as well as heterocycles containing nitrogen or sulfur. Zimmer and Schwartz GmbH (Germany) developed a complex binder based on a natural resin with additives of hydrocarbons of the paraffin and polyethylene series, fatty acids and an inorganic binder. This technology provides for efficient coating of the filler grains with the binder and produces a hydrophobic effect which makes it possible to achieve a hydration resistance level of up to 1 month without impregnation of the product.

An organic binder which is an amorphous plastic polymer of a new type with a silicon-carbon bond and improved heat resistance was developed in Japan. The polymer has a lattice structure, softening temperature above 300^0C and is soluble in xylene, hexane, and some other organic solvents. The binder has proved to be successful in refractories, including those of basic composition [18].

British researchers suggest a method for production of carbon-containing refractories in which the binder is a blend of polymers formed by homo-polymerization of resorcinol and isomers of dihydroxydiphenyl and trihydroxydiphenyl. The binder is a thermoplastic mixture with a softening temperature around 80^0C and is cured at 300^0C. This polymer is environmentally safe and is used for production of refractories based on chamotte, dolomite, corundum, periclase, silicon carbide and others, which exhibit good service properties.

There are new safe binders with a high coke residue available, including a thermosetting resin with cyclohexane or acetophenone as solvent, a phenol resin modified with a cyclic compound of alkyl ether or alkylbenzene with a solvent based on ketone ether, a mixture of phenol resin of the resol type with diethyl phtalate or furfural. An efficient complex binder based on carbomethoxy-substituted oligophenyl, synthetic resin, and amine compound which ensures the high strength of heat-treated articles in service has been developed. There are compositions with improved properties based on coal pitch and natural resins, such as a mixture of coal pitch and tar resin.

The new technologies for application of polymer resins largely determine the contemporary level of technical progress in production of refractories, corrosion-resistant ceramics, and composites. A special place belongs to thermosetting materials that do not contain phenol and do not release toxic agents in the course of their decomposition, and moreover the articles based on them have good operating characteristics. The development of materials based on combined oligomers makes it possible to reduce the consumption of materials in short supply, improve product quality, and improve the environmental conditions in production of engineering ceramics, refractories, including non-fired refractories, and fireproof polymer-ceramic composite materials.

References

[1] *Am. Ceram. Soc. Bull.,* 76(7), 95 - 100 (1997).

[2] C. Riesz & S. Susman, *"Synthetic binders for coke-graphite materials,"* Proc. 4th Conf. Carbon (1960), p. 609- 623.

[3] G. Veibel, P. Barta, & G. Waldhans, *"Properties and application of refractories based on polymer carbon binder,"* in: Ferrous Metallurgy in Russia and CIS Countries in XXI Century, Vol. 2, Metallurgiya, Moscow (1994).

[4] S. Miyagawa, M. Yokoi, & A. Mastuo, *"Refractories for cast-iron ladles,"* Ceram. Ing. Sci. Proc., 7, 58 - 74 (1986).

[5] B. I. Polyak, A. S. Vlasov, & O. A. Korehagina, *"Binders in the technology of silicon carbide ceramics,"* Tr Inst. MKhTI D. 1. Mendeleeva, Issue 137, 141 - 146 (1985).

[6] *Proc. Unified lnt. Techn. Conf. on Refractories "UNITECR '91",* Aachen (1991), pp. 73 - 75.

[7] *Graphite as a High-Temperature Material [Russian translation],* Mir, Moscow (1964).

[8] V. L. Balkevich, Engineering Ceramics, Slroiizdat, Moscow (1984).

[9] *Refractory Products and Materials: Reference Book [in Russian],* Metallurgiya, Moscow (1991).

[10] V. A. Kononov, *"State and prospects of refractory industry,"* Chem. Metal., Issue 2, 3 - 16 (1992).

[11] *Chemical Encyclopedia [in Russian],* Vol. 3, Bol'shaya Russkaya Entsiklopedia, Moscow (1992).

[12] G. D. Semchenko, *"Physicochemical processes occurring in heating of coal pitch and its mixtures with ethyl silicate,"* Ogneupory, No. 4, 14 - 18 (1997).

[13] M. I. Chudakov, Industrial Application of Lignin [in Russian], Lesnaya promyshlennost', Moscow (1983)

[14] V. P. Nedostvitskii, G. I. Antonov, M. A. Vinogradova, & L. K. Dimakova, *"Use of lignosulfonates as binders in the production of refractories,"* Ogneupory, No. 5, 7 - 11 (1994)

[15] A. Knop & V. Shveib, Phenol Resins and Materials Based on Them [in Russian], Khimiya, Moscow (1983)

[16] *Keram. Zeit. 40 (12),* 964 - 965 (1988).

[17] G. Zoglmeyr, *"Technical and envirornental aspects of the use of phenolic resins in modern-day refractories,"* lnterceram., 42(3), 145 - 149 (1993).

[18] *Chem. Chem. Technol.,* 40**,** 309-311 (1987).